1 **Organic geochemistry of the early Toarcian oceanic anoxic event in Hawsker**

2 **Bottoms, Yorkshire, England**

3

4 K. L. French[a*], J. Sepúlveda[b], J. Trabucho-Alexandre[c], D. R. Gröcke[c], R. E. Summons[b]

5

6 [a] Joint Program in Chemical Oceanography; Massachusetts Institute of Technology and

7 Woods Hole Oceanographic Institution, Cambridge, MA 02139, United States

8 [b] Department of Earth, Atmospheric, and Planetary Sciences; Massachusetts Institute of

9 Technology, Cambridge, MA 02139, United States

10 [c] Department of Earth Sciences, University of Durham, Durham, DH1 3LE, UK

11

12 *Corresponding author:

13　　　 E-mail address: klfrench@mit.edu (K. L. French)

14　　　 Tel: +01 617-324-3953

15 **Abstract**

16   A comprehensive organic geochemical investigation of the Hawsker Bottoms

17 outcrop section in Yorkshire, England has provided new insights about environmental

18 conditions leading into and during the Toarcian oceanic anoxic event (T-OAE; ~183 Ma).

19 Rock-Eval and molecular analyses demonstrate that the section is uniformly within the

20 early oil window. Hydrogen index (HI), organic petrography, polycyclic aromatic

21 hydrocarbon (PAH) distributions, and tricyclic terpane ratios mark a shift to a lower

22 relative abundance of terrigenous organic matter supplied to the sampling locality during

23 the onset of the T-OAE and across a lithological transition. Unlike other ancient intervals

24 of anoxia and extinction, biomarker indices of planktonic community structure do not

25 display major changes or anomalous values. Depositional environment and redox

26 indicators support a shift towards more reducing conditions in the sediment porewaters

27 and the development of a seasonally stratified water column during the T-OAE. In

28 addition to carotenoid biomarkers for green sulfur bacteria (GSB), we report the first

29 occurrence of okenane, a marker of purple sulfur bacteria (PSB), in marine samples

30 younger than ~1.64 Ga. Based on modern observations, a planktonic source of okenane's

31 precursor, okenone, would require extremely shallow photic zone euxinia (PZE) and a

32 highly restricted depositional environment. However, due to coastal vertical mixing, the

33 lack of planktonic okenone production in modern marine sulfidic environments, and

34 building evidence of okenone production in mat-dwelling Chromatiaceae, we propose a

35 sedimentary source of okenone as an alternative. Lastly, we report the first parallel

36 compound-specific $\delta^{13}C$ record in marine- and terrestrial-derived biomarkers across the

37 T-OAE. The $\delta^{13}C$ records of short-chain n-alkanes, acyclic isoprenoids, and long-chain n-

38   alkanes all encode negative carbon isotope excursions (CIEs), and together, they support

39   an injection of isotopically light carbon that impacted both the atmospheric and marine

40   carbon reservoirs. To date, molecular $\delta^{13}C$ records of the T-OAE display a negative CIE

41   that is smaller in magnitude compared to the bulk organic $\delta^{13}C$ excursion. Although

42   multiple mechanisms could explain this observation, our molecular, petrographic, and

43   Rock-Eval data suggest that variable mixing of terrigenous and marine organic matter is

44   an important factor affecting the bulk organic $\delta^{13}C$ records of the T-OAE.

45

1. Introduction

Several transient episodes of enhanced deposition and preservation of organic-rich sediments punctuated the Mesozoic Era. A combination of factors may have caused these intervals, known as oceanic anoxic events (OAEs), including greenhouse conditions and enhanced marine productivity (e.g. Schlanger and Jenkyns, 1976; Jenkyns, 1980; 1988; 2010; Trabucho-Alexandre et al., 2010). The first Mesozoic OAE was the Early Jurassic Toarcian OAE (T-OAE; ~183 Ma), which was associated with elevated extinction rates, enhanced weathering rates, warm temperatures, ocean acidification, and a negative carbon isotope excursion (CIE) (Hesselbo et al., 2000; Cohen et al., 2004; Bambach, 2006; Hesselbo et al., 2007; Jenkyns, 2010; Kiessling and Simpson, 2011). The duration of the T-OAE is not precisely known but may have lasted on the order of several hundred thousand years (Kemp et al., 2005; Suan et al., 2008; Kemp et al., 2011). The Karoo and Ferrar igneous provinces, which erupted at 183 ± 1 Ma, may have coincided with the Pliensbachian-Toarcian extinction (Pálfy and Smith, 2000; Courtillot and Renne, 2003). However, better radiometric dating of the volcanism and OAE are required to confidently link these two events. Although multiple mechanisms have been proposed to account for the Toarcian negative CIE, including methane hydrate dissociation, upwelling of isotopically light waters, thermogenic release of methane, and biomass burning (Hesselbo et al., 2000; Schouten et al., 2000; McElwain et al., 2005; van de Schootbrugge et al., 2005; Finkelstein et al., 2006), the source of the isotopically light carbon remains unclear.

70   The analysis of sedimentary organic matter provides the opportunity to evaluate

71   environmental and ecological responses to carbon cycle perturbations, as well as

72   potentially constraining the perturbation itself. Previous organic geochemical work across

73   the T-OAE has indicated changes in planktonic community structure and redox

74   chemistry, particularly the development of photic zone euxinia (PZE) (e.g. Farrimond et

75   al., 1989; 1994; Schouten et al., 2000; Pancost et al., 2004; Schwark and Frimmel, 2004;

76   Bowden et al., 2006; van Breugel et al., 2006). However, since biomarker records can

77   reflect local responses, additional comprehensive organic geochemical studies from

78   multiple locations are required to build a global perspective of ecological and

79   environmental change associated with the T-OAE. Here, we investigate the temporal

80   variation of lipid biomarkers, Rock-Eval data, organic petrography, and compound-

81   specific carbon isotopes from the Lower Jurassic section at Hawsker Bottoms, Yorkshire,

82   England.

83

84   **2.   Geologic Setting and Site Description of Hawsker Bottoms, Yorkshire, England**

85

86   A well-studied section of the Toarcian OAE is located on the Yorkshire coast in

87   northern England. We analyzed sample splits spanning 14 m of an organic-rich, lower

88   Jurassic outcrop section in the Cleveland Basin at Hawsker Bottoms previously studied

89   by Hesselbo et al. (2000). The lithology is dominated by black shales containing discrete

90   levels of calcite concretions and constitutes the Jet Rock *sensu stricto* (Hesselbo and

91   Jenkyns, 1995). The sections around Hawsker Bottoms have been used for defining the

92   ammonite biostratigraphy of the Toarcian (Howarth, 1992).

93   The Early Jurassic paleogeography of the area, although somewhat uncertain, is

94   depicted in published paleogeographic maps (e.g. Bradshaw et al., 1992). The Cleveland

95   Basin of North Yorkshire was part of a system of shallow epicontinental seas and small

96   extensional tectonic basins linked to the Central Graben via the Sole Pit Basin. The

97   region formed part of the broad epicontinental sea that covered much of northwest

98   Europe. Marine sedimentation was initiated during the Late Triassic, and a succession of

99   marine siliciclastic mudstones accumulated during the Early Jurassic.

100   The Grey Shale Member of the Whitby Mudstone Formation consists of

101   bioturbated, silty mudstones with beds of calcareous siderite concretions. The mudstones

102   have thin sharp-based beds, wave ripple, and starved ripple laminations (Wignall et al.,

103   2005; Ghadeer and Macquaker, 2011). Grain size and bioturbation intensity decrease

104   toward the top of the unit, and sediment color darkens. The Jet Rock Member consists of

105   dark, organic matter-rich, fissile mudstones with abundant ammonites and horizons of

106   calcareous nodules. The boundary between these two members of the Whitby Mudstone

107   Formation likely represents an increase in water depth in the basin.

108   The early Toarcian (*D. tenuicostatum* Zone) was a period of major basin

109   subsidence throughout England. Organic matter content fluctuates through the Grey

110   Shales, but increasing levels of organic matter are present from the *D. semicelatum*

111   Subzone to the *C. exaratum* Subzone (*H. falciferum* Zone). Minor shoaling cycles with

112   striped siltstone laminae suggest that water depths were on the order of tens of meters

113   (Powell, 2010). Similarly, sedimentary structures suggest deposition during storms by the

114   effects of waves (Wignall et al., 2005; Ghadeer and Macquaker, 2011). Thus, bottom

115   water conditions were more energetic than is commonly thought, where the water column

116   was likely shallower than 50 m. Consequently, Hawsker Bottoms likely represents an

117   inner continental shelf environment, which physical oceanographers define as the region

118   where turbulence from the surface and bottom boundary layers effectively homogenizes

119   the whole water column (Lentz and Fewings, 2012). Accordingly, inner shelf

120   environments are typically a few meters to tens of meters deep

121   The abundance of ammonites in the shales indicates that the water column was at

122   times oxygenated and favorable to nektonic faunas (Powell, 2010). The abundance of thin

123   beds with tops homogenized by bioturbation suggests that long-term, persistent bottom

124   water anoxia did not occur in the basin (Ghadeer and Macquaker, 2011). Besides

125   deposition as bedload by geostrophic flows and density currents, additional sediment was

126   supplied by suspension settling. Textural analyses have shown that much of the

127   sedimentary organic matter was delivered to the seafloor as fecal pellets, flocs, or other

128   organo-mineralic aggregates (Ghadeer and Macquaker, 2011). The contribution of a

129   biogenic component to rock composition varies, and the differences have been attributed

130   to a changing balance of primary production relative to dilution and length of transport

131   path during deposition (Macquaker and Taylor, 1996; Wignall et al., 2005; Ghadeer and

132   Macquaker, 2011).

133

134   **3. Methods**

135   Powdered rock samples were analyzed by Rock-Eval pyrolysis. The total organic

136   carbon (TOC; %), T_{max} (°C), S_1, and S_2 were determined and used to calculate the

137   hydrogen index (HI) and production index (PI). Kerogen isolates from four samples

138   across the section were mounted onto slides in duplicate and assessed optically under

139 white light and fluorescent light using a Zeiss research microscope and a Zeiss x 40

140 Plank-Neofluar objective. A Zeiss Axioskop, Axio Image D1, and a Zeiss 18 filter set

141 were used to take photomicrographs and fluorescence images.

142 Powdered samples (~ 5 g) were extracted using a Dionex ASE 200 Accelerated

143 Solvent Extractor with a solvent mixture of dichloromethane:methanol 9:1 (v/v).

144 Elemental sulfur was removed from the total lipid extract (TLE). Asphaltenes were

145 separated from the maltene fraction, which was then separated into saturated, aromatic,

146 and polar fractions by silica gel chromatography. The saturated and aromatic fractions

147 were analyzed by gas chromatography-mass spectrometry (GC-MS) and gas

148 chromatography-metastable reaction monitoring-mass spectrometry (GC-MRM-MS).

149 Carbon isotopic measurements of saturated hydrocarbons were made by gas

150 chromatography/combustion/ isotope ratio mass spectrometry (GC-C-IRMS) using a

151 ThermoFinnigan Delta Plus XP coupled to a ThermoFinnigan Trace GC. The mean value

152 of triplicate analyses are reported here in per mil (‰) relative to Vienna Pee Dee

153 belemnite (VPDB), and the standard deviation from the mean value was 0.4‰ or less. A

154 detailed description of methods is included in the supplementary online material (SOM).

155

156 **4. Results and Discussion**

157 *4.1 Rock-Eval analysis*

158 Rock-Eval results provided insight into the thermal maturity and type of organic

159 matter preserved in the Hawsker Bottoms sediments. The TOC percentage (Hesselbo et

160 al., 2000) was plotted for comparison with the HI, PI, and T_{max} (fig. 1). The narrow range

161 of the PI (0.11-0.18) and T_{max} (429-440°C) parameters indicate that thermal maturity is

162   uniform through the section and at the early stage of oil generation (Peters et al., 2005).

163   Molecular indices of thermal maturity further substantiate this conclusion (see section

164   4.2).

165   The HI data reveal that the type of organic matter undergoes a transition that

166   appears to coincide with a lithological transition from medium grey shale to dark grey

167   thin-bedded shale within the limitations of our sampling resolution. The low HI values

168   below -2.5 m are characteristic of type III kerogen, whereas the higher HI values above -

169   3 m are characteristic of type II kerogen (Peters et al., 2005). Type III kerogen is

170   dominated by either terrigenous or highly degraded organic matter, and type II kerogen is

171   typically derived from marine organic matter (Peters et al., 2005).

172   Published HI values from other T-OAE localities also increase across the

173   initiation of the CIE (Prauss et al., 1991; Schouten et al., 2000; Röhl et al., 2001;

174   Sabatino et al., 2009; Suan et al., 2011). Previous workers have attributed the HI

175   variability to different degrees of organic matter degradation under varying redox

176   conditions (Schouten et al., 2000; Röhl et al., 2001; Sabatino et al., 2009). Alternatively,

177   others have argued that the HI variability represents a shift in the composition of the

178   organic matter (Suan et al., 2011). Petrographic and molecular evidence for the presence

179   of plant-derived material in these sediments (see section 4.3) supports the conclusion that

180   lower HI values at the bottom of the section are due to a larger abundance of terrigenous

181   organic matter relative to marine organic matter.

182

183   *4.2 Molecular indicators of thermal maturity*

184   The thermal history of the section was further assessed according to molecular

185   thermal maturity parameters (fig. 2). The C_{31} hopane 22S/(22S+22R) ratio was constant

186   through the section and exhibited a narrow range between 0.58 and 0.59. A value of

187   ~0.55 represents the endpoint which is reached around the main phase of oil generation

188   (Peters et al., 2005). The C_{30} hopane βα/(βα+αβ) ratio ranged from 0.08 to 0.11, which is

189   close to values indicative of a mature source rock (Peters et al., 2005). The C_{29} sterane

190   ααα 20S/(20S+20R) ratio varied from 0.52 to 0.57, which is comparable to the endpoint

191   value of 0.52-0.55 (Peters et al., 2005). In summary, molecular thermal maturity

192   indicators corroborate the Rock-Eval results, further supporting a uniform thermal

193   maturity within the early window of oil generation.

194   Some biomarker-based thermal maturity parameters can be influenced by

195   additional factors such as source and diagenetic effects (Moldowan et al., 1986; Dahl et

196   al., 1993; Peters et al., 2005; Bennett and Olsen, 2007; French et al., 2012). Indeed, two

197   of the thermal maturity parameters presented in figure 2 exhibit some variation tracking

198   changes in lithology and source input, despite the multiple lines of evidence supporting

199   constant thermal maturity through the section. The Ts/(Ts+Tm) ratio, where Tm is C_{27} 17

200   α -trisnorhopane and Ts is C_{27} 18 α -trisnorhopane, varied from 0.41 to 0.59, whereas the

201   diasterane/sterane ratio of C_{27-29} compounds ranged from 1.08 to 1.44. Both ratios deviate

202   from a relatively constant pattern in the lower ~2 meters of the section. This pattern is

203   explained by changes in lithology and/or organic matter source input, which is consistent

204   with lower HI values and additional evidence supporting variable terrigenous organic

205   input (see section 4.3).

206

207   *4.3 Biomarker and petrographic evidence of terrigenous organic matter input*

208   A combination of molecular and petrographic analyses was performed to evaluate

209   the relative contribution of terrigenous organic matter through the sampling interval (fig.

210   3). Previous work has suggested a terrigenous source for C_{19} and C_{20} tricyclic terpanes,

211   which has led to the use of C_{19}/C_{23} and C_{20}/C_{23} tricyclic terpane ratios to identify input of

212   terrigenous organic matter (Noble et al., 1986; Peters et al., 2005). These two ratios

213   display higher values in the lowest part of the section and decrease after the lithological

214   transition at -2.5 meters, indicating relatively greater terrigenous organic matter input in

215   the lowermost part of the sampling interval.

216   A wide range of PAHs was detected in the Hawsker Bottoms samples, including

217   phenanthrene, fluoranthene, pyrene, benzo[a]anthracene, triphenylene, chrysene,

218   benzo[b]fluoranthene, benzo[k]fluoranthene, benzo[e]pyrene, indeno[c,d]pyrene,

219   dibenzo[a,h]anthracene, benzo[g,h,i]perylene, coronene, and retene. PAHs are a diverse

220   set of compounds with multiple documented sources including products of pyrolysis,

221   combustion, hydrothermal activity, and igneous intrusion as well as direct inputs from

222   algae, fungi, vascular plants, and extraterrestrial organics (Kawka and Simoneit, 1990;

223   George, 1992; Jiang et al., 2000; Sephton et al., 2005; Grice et al., 2007; Marynowski and

224   Simoneit, 2009). PAHs have been used to reconstruct the history of wildfires, higher

225   plant input, and anthropogenic activity, where peri-condensed, unsubstituted PAHs are

226   markers for combustion of organic matter (Hites et al., 1977; Venkatesan and Dahl, 1989;

227   Killops and Massoud, 1992; Kruge et al., 1994; Jiang et al., 1998; Arinobu et al., 1999;

228   Finkelstein et al., 2005; Peters et al., 2005; Marynowski and Simoneit, 2009). Some

229   sedimentary PAHs, such as phenanthrene, chrysene, and triphenylene, are more affected

230   by diagenesis or additional sources (Jiang et al., 1998; Grice et al., 2007), so they were

231   not included in the total PAH sum plotted in figure 3b. Although the patterns are not

232   identical, enhanced concentrations of total PAH co-occur with elevated C_{19}/C_{23} and

233   C_{20}/C_{23} tricyclic terpane ratios in the bottom 2 meters of the sampling interval. Some

234   PAHS, such as retene, are thought to derive from higher plants, in particular coniferous

235   resin (Wakeham et al., 1980; Ellis et al., 1996; Jiang et al., 1998; Grice et al., 2005;

236   Peters et al., 2005), although algal and bacterial sources have been reported as well (Wen

237   et al., 2000). Retene was detected in all samples, and its concentration was plotted

238   separately as a marker of higher plant input in figure 3c. Retene was more abundant in

239   the lowest interval of the section, which is consistent with the total PAHs, tricyclic

240   terpane ratios, and HI data.

241   Microscopic analysis of four kerogen samples adds an additional line of evidence

242   supporting stratigraphic variations in kerogen type and organic matter sources. According

243   to the petrographic results, the kerogen is comprised of as much as 80% of terrigenous

244   organic matter in the bottom of the section and about 25-40% in the remainder of the

245   sampling interval (fig. 3d). Since the elemental, molecular, and isotopic composition of

246   organic matter from higher plants is distinct from marine organic matter, HI can reflect

247   the compositional difference of distinct types of organic matter (e.g. Talbot and

248   Livingstone, 1989). Assuming constant HI values for terrigenous and marine organic

249   matter end-members, the percent terrigenous organic matter was estimated through the

250   section using the linear relationship between the percent terrigenous macerals measured

251   by optical microscopy and the corresponding HI (see SOM for more details). Calculated

252   values of $f_{Terr\,OM}$ ranged from 12 to 85%, where the highest values were found in the

253   lowermost part of the section (fig. 3e).

254   The stratigraphic change in the relative supply of terrigenous organic matter ,

255   which is supported by the HI, molecular, and petrographic results, may have been driven

256   by effects related to rising sea level (Hesselbo, 2008; Suan et al., 2011). Considering that

257   increased rates of continental weathering across the T-OAE would have enhanced

258   delivery of terrigenous material (Cohen et al., 2004), the opposite trend recorded in our

259   data might be best explained by progressive remoteness from the coastline on a gently

260   sloping shelf during sea level transgression (e.g. Macquaker et al., 2010). However, sea

261   level related effects might not be the only factor responsible for the changing signal in

262   relative abundance of terrigenous and marine organic matter. For example, enhanced

263   marine export productivity and/or enhanced marine organic matter preservation could

264   have diluted the input of terrigenous organic matter, thereby changing the relative

265   apparent contribution.

266

267   *4.4 Biomarker indicators of source and community structure*

268   Since some compounds or compound classes are associated with a particular

269   biological source, metabolism, or physiology, molecular distributions can be informative

270   about changes in microbial community structure. Unlike other intervals of ocean anoxia

271   associated with mass extinction events (e.g. Xie et al., 2005; Cao et al., 2009), algal- and

272   bacterial-derived biomarkers indicative of community structure did not vary significantly

273   through the CIE (fig. 4). Instead, some biomarker indices that typically reflect

274   community structure were more affected by source input at Hawsker Bottoms.

275   The regular sterane/17α-hopane ratio is used as an indicator of the relative

276   contributions of eukaryote and bacterial biomass. The regular sterane/hopane ratio was

277   calculated using regular C_{27-29} steranes and 17α C_{29-33} hopanes. The regular sterane/17α-

278   hopane ratio exhibited low values below -2.5 m, whereas it was more elevated (>0.5) and

279   relatively constant in the top 10 m of the section. While this offset could be interpreted as

280   a shift from a bacterially dominated environment in the lower part of the section to a

281   eukaryotic environment above -3 m, it is more likely that a change in the organic matter

282   source input is driving the regular sterane/17α-hopane ratio variability. As well as

283   containing low total steroid abundances, terrigenous organic matter can deliver hopanes

284   derived from soil bacteria, thereby lowering the regular sterane/17α-hopane ratio (Peters

285   et al., 2005; Handley et al., 2010; Sãenz et al., 2011; French et al., 2012).

286   Similarly, small deviations are found at the bottom of the section for the C_{27}/C_{27-}

287     $_{30}$, C_{28}/C_{27-30}, and C_{29}/C_{27-30} sterane ratios. These ratios included regular steranes as well

288   as diasteranes and are commonly used as indicators of the relative contribution from red

289   algae biomass, chlorophyll-c algae, and green algae, respectively. However, they can also

290   be affected by the delivery of C_{29} steranes derived from land plants (Moldowan et al.,

291   1985; Peters et al., 2005). Indeed, C_{29} sterane was the dominant sterane in samples from

292   the bottom of the section, where it represented nearly half of the total C_{27-30} steranes. The

293   C_{30}/C_{27-30} sterane ratio, on the other hand, which is an indicator of marine pelagophyte

294   algae, was constant throughout the section and represented only a minor proportion of the

295   total steranes abundance.

296   The 2α-methylhopane index (2-MHI) has been used as an indicator of

297   cyanobacterial input (Summons et al., 1999), although additional sources were later

298   reported (Rashby et al., 2007). The 3β-methylhopane index (3-MHI) is considered a

299   marker for aerobic proteobacteria, including methanotrophs and acetic acid bacteria

300   (Zundel and Rohmer, 1985; Talbot et al., 2003; Farrimond et al., 2004; Talbot and

301   Farrimond, 2007). The 2-MHI and 3-MHI were invariant, and the 3-MHI was in the

302   range of average Phanerozoic marine values (~1-3%) (Farrimond et al., 2004; Cao et al.,

303   2009). Likewise, the 2-MHI also lacked elevated values. Based on elevated 2-MHI, 3-

304   MHI, and nitrogen isotope anomalies, previous workers have reported an increased

305   contribution of diazotrophic cyanobacteria and methanotrophic bacteria during other

306   OAEs (e.g. Kuypers et al., 2004; Cao et al., 2009; Sepúlveda et al., 2009; Luo et al.,

307   2011). The low and invariant contribution of these microbial groups indicates that

308   environmental conditions suitable for their predominance did not prevail at this locality.

309   Thus, enhanced cyanobacterial diazotrophy may not fully explain the previously reported

310   depleted bulk organic $\delta^{15}N$ at this location during the T-OAE (Jenkyns et al., 2001).

311

312   *4.5 Indicators of redox change and depositional environment*

313   A suite of biomarkers was used to assess changes in water column stratification

314   and redox potential, including the gammacerane index, C_{35} homohopane index (C_{35} HHI),

315   pristane/phytane (Pr/Ph) ratio, and the concentration of aromatic carotenoid derivatives

316   (fig. 5). Although some of these parameters can also be influenced by diagenesis, source

317   input, and thermal maturity, they display patterns consistent with a shift towards more

318   intense reducing conditions at least in the sediment porewaters and potentially in the

319   overlying water column.

320   Although the biological sources of gammacerane are not fully known (Peters et

321 al., 2005), it is a diagenetic product of tetrahymanol, a compound found in bacteriovorous

322 ciliates thriving at the chemocline of stratified water bodies (ten Haven et al., 1989;

323 Sinninghe Damsté et al., 1995). Thus, the occurrence of gammacerane, expressed as the

324 gammacerane index = *[gammacerane/ (gammacerane + 17α,21β C$_{30}$ hopane)]*100,* has

325 been used to infer changes in water column stratification in ancient environments.

326 Gammacerane was detected in all of the analyzed samples but became more prominent in

327 those deposited during the OAE, starting at the onset of thin-bedded shales.

328   Elevated abundances of gammacerane during the T-OAE may reflect the

329 development of seasonal water column stratification, possibly due to stronger seasonality

330 and/or deepening of the water column. In contrast, prior to the T-OAE, seasonality may

331 have been weaker, or the water column may have been too shallow to stratify, even

332 during warm months, due to turbulent mixing. The development of seasonal water

333 column stratification at Hawsker Bottoms during the T-OAE would have aided the

334 development of water column oxygen-depletion, particularly during warm and productive

335 months. However, gammacerane enrichments alone do not necessitate water column

336 anoxia, particularly given the association of its precursor, tetrahymanol, with suboxic

337 waters in the modern (Wakeham et al., 2007; 2012).

338   The C$_{35}$ HHI and Pr/Ph ratio are recorders of depositional redox conditions in

339 sediments. The C$_{35}$ HHI records the degree of preservation of the extended side chain of

340 C$_{35}$ hopanes derived from intact bacteriohopanepolyols (BHPs) (Köster et al., 1997;

341 Peters et al., 2005). Higher C$_{35}$ HHI values are characteristic of oxygen-depleted marine

342 depositional environments. Pristane and phytane in ancient marine rock extracts and oils

343   are largely, but not exclusively, derived from the chlorophyll phytyl side chain from

344   photoautotrophs. Redox conditions influence the diagenetic pathway of the phytyl side

345   chain. Reducing conditions promote the conversion of phytol to phytane, and oxic

346   conditions promote the conversion of phytol to pristane (Didyk et al., 1978; Peters et al.,

347   2005). The C_{35} HHI nearly doubled in samples deposited during the OAE compared to

348   those deposited prior to the event. Values of the Pr/Ph ratio >3 recorded at the bottom of

349   the section are suggestive of deposition of terrigenous organic matter under oxic

350   conditions. The Pr/Ph ratio values near or below 1 during the T-OAE, together with the

351   elevated C_{35} HHI, suggest intensification of reducing conditions in the sediment

352   porewaters during deposition.

353   Biomarkers for anaerobic phototrophic green sulfur bacteria (GSB) have been

354   used to argue for the development of PZE during the T-OAE (Schouten et al., 2000;

355   Pancost et al., 2004; Bowden et al., 2006) and other OAEs (e.g. Cao et al., 2009) based

356   on the physiological requirement of co-occurring reduced sulfur species and light. We

357   detected 2,3,6-aryl isoprenoids, isorenieratane, and chlorobactane in all samples. Unlike

358   previous studies of the T-OAE or any Phanerozoic organic geochemical study of marine

359   samples, trace concentrations of okenane were also identified by GC-MRM-MS in

360   samples above -3 m, whereas it was below detection limit in samples from the lowest 2

361   meters of the section. Okenone, a photosynthetic pigment belonging to the PSB family

362   Chromatiaceae, is the only known precursor of okenane (Brocks and Schaeffer, 2008).

363   All compounds were compared with an authentic carotenoid standard and an extract from

364   the Barney Creek Formation (BCF; fig. 6; Brocks et al., 2005). Normalizations of the C_{40}

365   aromatic carotenoid derivatives against the mass of TOC and TLE reveal a similar pattern

366   of elevated concentrations during the anoxic event compared to the pre-event baseline.

367   In total, all of the organic geochemical redox indicators point towards a shift

368   towards more reducing conditions broadly corresponding with the initiation of the

369   negative CIE. However, sedimentological features, such as starved wave and combined

370   flow ripples, indicate that this area was an energetic, shallow inner shelf environment on

371   the order of tens of meters and probably no deeper than 50 m, where enough oxygen was

372   present in the water column on some timescale to sustain nektonic fauna, including

373   ammonites, and allow for bioturbation at the sediment-water interface through the OAE

374   (Wignall et al., 2005; Powell, 2010; Ghadeer and Macquaker, 2011). We explore

375   different scenarios to reconcile these apparent opposing lines of evidence.

376   First, the geochemical and sedimentological signals recorded in the rock record

377   are a composite of many processes occurring on different timescales. In the modern

378   ocean, highly productive coastal and continental margin sediments and the overlying

379   water column oscillate between oxic and anoxic conditions over different timescales (e.g.

380   Burdige, 2007). Enhanced productivity and export of organic matter, which are important

381   features of Mesozoic OAEs (e.g. Erba, 2004; Jenkyns, 2010), would have increased the

382   oxygen demand in the water column and sediment porewaters during productive months.

383   During the T-OAE, anoxic conditions may have been restricted to the sediment

384   porewaters during seasons of low productivity, allowing bioturbation to occur when

385   bottom waters were better oxygenated. Conversely, oxygen-deficient waters may have

386   expanded seasonally to the water column during intervals of high productivity and

387   enhanced stratification, as implied by the gammacerane index.

388   Second, the molecular, paleontological, and sedimentary indicators of redox

389 chemistry apply to different parts of the depositional environment, diagenetic pathways,

390 and have different sensitivities along the redox spectrum. With the exception of the GSB

391 and PSB carotenoid markers, the geochemical parameters reported here do not require

392 strict anoxia or euxinia in the water column. The gammacerane index pattern supports the

393 development of seasonal stratification during the OAE, which would have promoted

394 oxygen depletion of the water column. However, the possibility remains that even during

395 intervals of high productivity and stratification, water column oxygen concentrations at

396 this location were depleted but high enough to sustain organisms with physiological

397 oxygen requirements, thereby explaining the fossil and sedimentary evidence.

398 Additionally, the Pr/Ph ratio and C_{35} HHI pertain primarily to sedimentary redox

399 conditions opposed to water column redox structure. Therefore, the occurrence of intact

400 aromatic carotenoid derivatives merits further discussion to assess water column redox

401 chemistry.

402   To date, okenane has only been reported in Paleoproterozoic rock extracts and

403 lacustrine Cenozoic extracts (Brocks et al., 2005; Zhang et al., 2011). Given the

404 atmospheric $p\mathrm{O}_2$ during the Mesozoic was near present atmospheric levels (Berner,

405 2006), its detection in marine samples of this age requires careful interpretation. The PSB

406 family Chromatiaceae blooms in a range of anoxic environments with light and reduced

407 sulfur species, including stratified lakes, fjords, coastal lagoons, estuaries, and coastal

408 microbial mats, but not all Chromatiaceae produce okenone (Brocks and Schaeffer, 2008

409 and references therein). Okenone-producing planktonic Chromatiaceae dwell in water

410 columns where the chemocline is above 25 m and in 75% of the reported cases less than

411   12 m (Brocks and Schaeffer, 2008). Notably, all of the modern chemocline depth

412   observations for okenone production are based on stratified lake systems. Thus, the lack

413   of okenone in modern marine sulfidic environments presents a "no analogue problem" for

414   ancient marine samples containing okenane that were deposited under atmospheric pO_2

415   close to modern levels.

416   Transient free sulfide has been reported in the water column of intense upwelling

417   zones, including the Arabian Sea, Namibian coast, and the Peruvian coast (e.g Dugdale et

418   al., 1977; Brüchert et al., 2003; Naqvi et al., 2006; Schunck et al., 2013). However, these

419   episodes are typically short lived. In contrast, sulfidic waters persist in some restricted

420   marine basins and fjords, including the Black Sea, Cariaco Basin, Saanich Inlet, and the

421   Framvaren and Effingham Fjords. However, these two types of marine environments

422   (non-restricted, transiently sulfidic and restricted, permanently sulfidic) fail to represent

423   suitable modern analogues for Hawsker Bottoms on several counts. Isorenieratene has

424   been measured in the water column and sediments of some restricted marine basins,

425   particularly fjords and the Black Sea (e.g. Sinninghe Damsté and Schouten, 2006), but

426   GSB carotenoids have not been detected in transiently sulfidic upwelling systems.

427   Furthermore, okenone has not been reported in the water column or sediments of any

428   modern marine transiently or permanently sulfidic environment, with the exception of the

429   upper sediments of Kyllaren fjord, a small, highly restricted basin (Smittenberg et al.,

430   2004; Sinninghe Damsté and Schouten, 2006). Like okenone, modern planktonic marine

431   occurrences of chlorobactene are also limited to semi-enclosed water masses that are not

432   representative of fully marine conditions (e.g. Naeher et al. 2012). Interestingly, multiple

433   emerging lines of evidence suggest the occurrence of a "cryptic sulfur cycle" in some

434 OMZs, with a potential role for photosynthetic sulfide oxidation (Canfield et al., 2010;

435 Stewart et al., 2012). However, the presence of GSB and/or PSB and their respective

436 carotenoids have yet to be reported in modern OMZs.

437   Furthermore, the physical oceanographic processes determining the degree of

438 vertical mixing, hence stratification and redox gradient stability, are markedly different

439 between inner shelf environments and sulfidic, silled basins, which are highly restricted

440 and in many classic modern examples, are an order of magnitude or more deeper than

441 estimated paleodepths of Hawsker Bottoms. Although the water column at Hawsker

442 Bottoms became deeper with the sea level transgression across the T-OAE, the

443 depositional environment remained relatively shallow because of its location on a gently

444 sloping shelf (e.g. Macquaker et al., 2010). Consequently, turbulent mixing at the surface

445 and bottom boundary layers would have prevented a stable sulfidic chemocline from

446 developing. On the other hand, considering the limited occurrence of planktonically

447 produced okenone in modern lakes, a planktonic source of okenone at Hawsker Bottoms

448 would imply that, rather than an inner shelf environment, Hawsker Bottoms was a highly

449 restricted coastal basin not reflective of fully marine conditions.

450   Alternatively, we argue that okenane at Hawsker Bottoms was likely derived from

451 benthic microbial mats based on the lack of modern analogues of okenone-production in

452 marine sulfidic environments, the dynamics of inner shelf physical mixing, and building

453 evidence of okenone-producing, mat-dwelling Chromatiaceae (e.g. Caumette et al., 1991;

454 Airs et al., 2001; Caumette et al., 2004; Meyer et al., 2011). Furthermore, planktonic

455 Chlorobiaceae are not the exclusive source of isorenieratene and chlorobactene. Previous

456 work has documented additional non-planktonic GSB sources of isorenieratene and

457   chlorobactene, including microbial mats (e.g.Wahlund et al., 1991; Brocks and

458   Summons, 2003; Beatty et al., 2005; Bühring et al., 2011). Although a mixed planktonic

459   and mat origin of the carotenoids cannot be ruled out, it is more likely that the GSB and

460   PSB carotenoids detected in Hawsker Bottoms samples share a source. Previous studies

461   of sedimentary structures in the Toarcian shales of Yorkshire have attributed wavy

462   laminations to microbial mats (O'Brien, 1990), thereby further supporting a sedimentary

463   origin of GSB and PSB carotenoid derivatives detected in Hawsker Bottoms samples.

464   Similar wavy laminated fabrics have been reported in coeval shales in northern European

465   T-OAE sections (Trabucho-Alexandre et al., 2012). Unfortunately, a sedimentary source

466   of the GSB and PSB carotenoid derivatives offers little information about water column

467   redox chemistry. However, this interpretation does not preclude the development of a

468   suboxic, anoxic, or euxinic water column in this region on some timescale during the T-

469   OAE. Instead, additional inorganic geochemical data is required to better assess the water

470   column redox conditions and degree of basin restriction (Algeo and Tribovillard, 2009).

471

472   *4.6 Compound specific stable carbon isotopic data*

473   A limited number of compound specific $\delta^{13}C$ records of the T-OAE are currently

474   available in the literature. Here, we report the first long-chain *n*-alkane $\delta^{13}C$ records of

475   the T-OAE. Compound specific $\delta^{13}C$ analyses of marine- and terrestrial-derived lipids

476   reveal a shift towards lighter $\delta^{13}C$ values (fig. 7). Short-chain *n*-alkanes, as well as

477   pristane and phytane are typically used as marine indicators, whereas long-chain *n*-

478   alkanes primarily reflect terrigenous sources. The *n*-C_{17}, *n*-C_{18}, and *n*-C_{19} alkanes

479   displayed a negative excursion of ~2–3‰, which is consistent with the ~2–4‰ negative

480   excursions documented in the partial n-C_{16-20} alkane records from the Toarcian

481   Posidonienschiefer in southwest Germany (Schouten et al., 2000). Pristane and phytane

482   encode a muted excursion (~1.5–2‰) compared to short-chain alkane records, and they

483   also have smaller CIE magnitudes compared to the pristane and phytane isotopic records

484   from the Toarcian Paris Basin and the Posidonienschiefer (~3–4‰) (Schouten et al.,

485   2000; van Breugel et al., 2006). On the other hand, long-chain n-alkanes (n-C_{27}, n-C_{28},

486   and n-C_{29}), which are primarily but not exclusively derived from epicuticular waxes of

487   vascular plants (Eglinton and Hamilton, 1967), display the largest compound specific

488   negative CIE (~4–5‰). The molecular isotopic records appear to register the initiation of

489   the negative CIE earlier than in the bulk organic record, and within the CIE, the

490   compound-specific $\delta^{13}C$ values remain fairly stable while the bulk curve becomes

491   gradually depleted. However, these features could be due to sampling resolution

492   differences. Higher resolution molecular isotopic records are required to better address

493   the timing and structure of the isotopic excursion recorded in different carbon reservoirs.

494   The absolute magnitude of the bulk organic CIE (~5–7‰) is larger than the CIEs

495   recorded in the molecular records from Yorkshire (this study; ~1.5–5‰), the Paris Basin

496   (~3‰; van Breugel et al., 2006), and the Posidonienschiefer (~2–4‰; Schouten et al.,

497   2000). Identifying the reason behind the CIE magnitude offsets is critical for placing

498   bounds on the magnitude of isotopically light carbon added into the system. Bulk organic

499   matter is comprised of an array of molecularly and isotopically heterogeneous

500   constituents. In addition to environmental perturbations, organic matter source mixing

501   can contribute to bulk organic $\delta^{13}C$ excursions (e.g. Pancost et al., 1999). The comparison

502   of short- and long-chain n-alkane isotopic compositions demonstrates that, unlike the

503   modern, terrigenous organic matter is isotopically heavier than marine organic matter

504   during the Toarcian (fig. 7), which is consistent with previous Toarcian studies (Vetö et

505   al., 1997; Schouten et al., 2000). Multiple lines of evidence presented in section 4.3

506   highlight a significant transition in the terrigenous organic matter input at Hawsker

507   Bottoms. Indeed, the bottom 2 meters of the study interval are dominated by terrigenous

508   organic matter and are isotopically heavier than the overlying interval that is dominated

509   by marine organic matter. Therefore, an undetermined component of the bulk organic

510   CIE magnitude may be attributed to source mixing effects.

511   Additional factors could also contribute to the difference in magnitudes between

512   bulk and molecular CIEs. For instance, it is possible that the full CIE was not captured in

513   the molecular isotopic records due to a lower sampling resolution compared to the bulk

514   organic δ^{13}C records. Alternatively, water availability can modulate the magnitude of the

515   CIE recorded in vascular leaf waxes, as has been discussed for the Paleocene Eocene

516   Thermal Maximum (PETM; e.g. Schouten et al., 2007; Smith et al., 2007), but unlike the

517   PETM, the ratio of angiosperms and conifers would not account for the *n*-alkane and bulk

518   organic CIE magnitude offset because the rise of angiosperms postdates the Early

519   Jurassic (e.g. Heimhofer et al., 2005). Additionally, thermal maturation could influence

520   the δ^{13}C of individual compounds, which become isotopically heavier with increasing

521   thermal maturity (Clayton, 1991; Clayton and Bjorøy, 1994; Tang et al., 2005).

522   Nevertheless, while multiple mechanisms may account for the difference between

523   molecular and bulk organic CIE magnitudes, it is significant that a negative CIE is

524   recorded in both marine- and terrestrial-derived lipids, albeit to different degrees. The

525   parallel isotopic change in marine and terrestrial carbon pools recorded at Hawsker

526 Bottoms further supports previous studies suggesting that the T-OAE was a global carbon

527 cycle perturbation where isotopically light carbon entered the atmospheric, terrigenous,

528 and marine carbon reservoirs (Hesselbo et al., 2000; 2007; Al-Suwaidi et al., 2010;

529 Caruthers et al., 2011; Gröcke et al., 2011). Multiple sources of isotopically light carbon

530 have been proposed, including methane hydrate dissociation, regional upwelling of

531 isotopically light waters in stratified epicontinental seas, thermogenic release of methane

532 from organic-rich strata in contact with dykes, biomass burning, or a combination of

533 these mechanisms (Hesselbo et al., 2000; Schouten et al., 2000; McElwain et al., 2005;

534 van de Schootbrugge et al., 2005; Finkelstein et al., 2006).

535   Although our study does not provide evidence in support of a specific forcing

536 mechanism, it allows us to narrow down potential mechanisms. A deep-water source of

537 isotopically light carbon is unlikely because of the CIE observed in land plant

538 biomarkers. The lack of evidence for bacterial methanotrophy in our section suggests that

539 methane hydrate dissociation did not supply appreciable methane to the sampling

540 locality. The organic matter source transition complicates the interpretation of PAH

541 abundances as tracers of biomass burning, so a different sampling locality without an

542 organic matter source transition should be studied to test the biomass burning mechanism

543 using PAHs. A cascade of mechanisms rather than a single mechanism likely initiated the

544 T-OAE. However, our results indicate that the influence of source mixing on the bulk

545 organic $\delta^{13}C$ has been previously underestimated and could have potentially affected

546 other bulk isotopic systematics such as nitrogen. Therefore, previous estimates regarding

547 the magnitude of this global perturbation of the carbon cycle should be revisited.

548

5. Conclusions

We use a multiproxy approach based on bulk geochemistry, lipid biomarkers, and compound-specific stable isotopes to elucidate environmental and ecological changes associated with the T-OAE at Hawsker Bottoms in Yorkshire, England. Molecular indicators and Rock-Eval results suggest that thermal maturity is uniformly in the early oil generation window throughout the sampling interval. The HI data, organic petrography, PAH distribution, and tricyclic terpane ratios indicate a transition in the relative input of terrigenous vs. marine organic matter across a lithological transition. The shift to lower relative abundance of terrigenous organic matter was likely a result of sea level related effects such as coastal proximity, changes in marine organic matter preservation, and/or dilution effects from increased marine productivity.

Organic geochemical redox and depositional environment indicators point towards an overall shift towards more reducing conditions in sediment porewaters and the development of seasonal stratification during the OAE. Previous sedimentological observations require that the water column was not completely anoxic throughout the entire T-OAE, which may seem contradictory at first to the detection of GSB and PSB carotenoids. However, here we present the first occurrence of okenane, a carotenoid marker of PSB, in marine samples younger than the Paleoproterozoic (1.64 Ga). This unexpected finding challenges the interpretation of GSB and PSB carotenoids as markers of PZE in the context of Hawsker Bottoms due to inner shelf vertical mixing, the lack of modern analogues of okenone-production in marine sulfidic environments, and the emerging evidence of okenone-producing mat-dwelling Chromatiaceae. Therefore, in combination with previous reports of microbial wavy lamination in Toarcian shales of

572   Yorkshire and coeval shales in northern Europe, we argue that okenane, and potentially

573   chlorobactane and isorenieratane, was most likely mat-derived at Hawsker Bottoms.

574   The compound-specific $\delta^{13}C$ records of short-chain n-alkanes, acyclic

575   isoprenoids, and long-chain n-alkanes support a carbon cycle perturbation that affected

576   both the atmospheric and marine systems, which precludes the recycling of isotopically

577   light CO_2 from anoxic waters as the sole mechanism responsible for the T-OAE negative

578   CIE. Notably, compound specific $\delta^{13}C$ records of the T-OAE, including the new data

579   presented here from Yorkshire and previous molecular data from the Paris Basin and the

580   Posidonienschiefer, encode negative CIEs that are smaller in magnitude compared to bulk

581   organic $\delta^{13}C$ records. Many mechanisms could contribute to this observation, particularly

582   variable mixing of terrigenous and marine organic matter, which is supported by the

583   multiple lines of evidence for a transition in organic matter source. Identifying the

584   mechanisms behind the CIE magnitude offsets is important for estimating the magnitude

585   of isotopically light carbon injected into the surface carbon reservoirs.

586

587   Acknowledgements

596

597   Figure Captions:

598   **Fig. 1. Rock-Eval Analysis. A)** Total organic carbon (TOC; %) (Hesselbo et al., 2000);
599   B) Hydrogen index (HI; mg HC/g TOC); C) Production index (PI); D) T_{max} (°C).
600
601   **Fig. 2. Molecular Indicators of Thermal Maturity**. A) The C_{31} hopane 22S/(22S+22R)
602   ratio; B) C_{30} hopane βα/(βα+αβ) ratio; C) C_{29} sterane ααα 20S/(20S+20R) ratio; D)
603   Ts/(Ts+Tm) ratio; E) diasteranes/steranes ratio. Note the lack of variation in A, B and C
604   across the section compared to the minor variations exhibited by D and E due to changes
605   in source input and/or lithology.
606
607   **Fig 3. Terrigenous Organic Matter Indicators**. A) Ratios of C_{19}/C_{23} and C_{20}/C_{23}
608   tricyclic terpanes; B) total concentration of PAHs normalized by TOC and TLE; C)
609   concentration of retene normalized by TOC and TLE; D) measured contribution of
610   terrigenous organic matter (OM) by petrographic analysis; E) calculated percentage of
611   terrigenous organic matter ($f_{Terr\ OM}$) based on linear regression ($f_{Terr\ OM}$ (%) = -0.279 * HI
612   + 136; R^2=0.90) of petrographic measurements of terrigenous organic matter (Fig. 3D)
613   and HI (Fig. 1B).
614
615   **Fig. 4. Source and Community Indicators**. A) The ratio of regular steranes/17α-
616   hopanes; B) C_{27}/C_{27-30} steranes; C) C_{28}/C_{27-30} steranes; D) C_{29}/C_{27-30} steranes; E) 2α-
617   methylhopane and 3β-methylhopane indices.
618
619   **Fig. 5. Redox and Depositional Environmental Indicators**. A) Gammacerane index; B)
620   C_{35} homohopane index (C_{35}HHI); C) pristane/phytane (Pr/Ph) ratio; D) concentration of
621   isorenieratane; E) concentration of chlorobactane; F) concentration of okenane. The
622   concentrations of C_{40} carotenoids are semi-quantitative and were normalized against TOC
623   and TLE.
624
625   **Fig. 6 Gas chromatography - metastable reaction monitoring - mass spectrometry**
626   **(GC-MRM-MS) chromatogram for the identification of aromatic carotenoid**
627   **derivatives.** MRM chromatograms displaying the 554→134 transition characteristic for
628   chlorobactane and okenane in an authentic standard of combined C_{40} carotenoids (A) and
629   in sample ENR004 at 5.98 m (C). Plots B and D are MRM chromatograms displaying the
630   546→134 MRM transition characteristic of isorenieratane, renieratane, and
631   renierapurpurane in an authentic standard of combined C_{40} carotenoid (B) and in sample
632   ENR004 (D). Compound abbreviations were used for labels: chlorobactane (Ch);
633   okenane (Ok); isorenieratane (Iso); renieratane (Ren); renierapurpurane (Rpurp).
634

635   **Fig. 7 Carbon Isotopic records**. A) Previously reported $\delta^{13}C_{org}$ from Hawsker Bottoms
636   (Hesselbo et al., 2000; Kemp et al., 2005); B) $\delta^{13}C$ of n-$C_{17\text{-}19}$ short-chain n-alkanes; C)
637     $\delta^{13}C$ of pristane and phytane; D) $\delta^{13}C$ of n-$C_{27\text{-}29}$ long-chain n-alkanes. Note the different
638   x-axis scales.
639

640   References
641

642   Airs, R.L., Atkinson, J.E., Keely, B.J., 2001. Development and application of a high
643   resolution liquid chromatographic method for the analysis of complex pigment
644   distributions. J. Chromatogr. A 917, 167–177.
645   Algeo, T. J., Tribovillard, N., 2009. Environmental analysis of paleoceanographic
646   systems based on molybdenum-uranium covariation. Chem. Geol. 268, 211-225.
647   Al-Suwaidi, A.H., Angelozzi, G.N., Baudin, F., Damborenea, S.E., Hesselbo, S.P.,
648   Jenkyns, H.C., Mancenido, M.O., Riccardi, A.C., 2010. First record of the Early
649   Toarcian Oceanic Anoxic Event from the Southern Hemisphere, Neuquén Basin,
650   Argentina. J. Geol. Soc. (London) 167, 633–636.
651   Arinobu, T., Ishiwatari, R., Kaiho, K., Lamolda, M.A., 1999. Spike of pyrosynthetic
652   polycyclic aromatic hydrocarbons associated with an abrupt decrease in $\delta^{13}C$ of a
653   terrestrial biomarker at the Cretaceous-Tertiary boundary at Caravaca, Spain.
654   Geology 27, 723–726.
655   Bambach, R.K., 2006. Phanerozoic biodiversity mass extinctions. Annu. Rev. Earth
656   Planet. Sci. 34, 127–155.
657   Beatty, J., Overmann, J., Lince, M., Manske, A., Lang, A., Blankenship, R., Van Dover,
658   C., Martinson, T., Plumley, F., 2005. An obligately photosynthetic bacterial anaerobe
659   from a deep-sea hydrothermal vent. Proc. Natl. Acad. Sci. U.S.A 102, 9306–9310.
660   Bennett, B., Olsen, S., 2007. The influence of source depositional conditions on the
661   hydrocarbon and nitrogen compounds in petroleum from central Montana, USA. Org.
662   Geochem. 38, 935–956.
663   Berner, R., 2006. GEOCARBSULF: A combined model for Phanerozoic atmospheric O_2
664   and CO_2. Geochim. Cosmochim. Acta 70, 5653–5664.
665   Bowden, S.A., Farrimond, P., Snape, C.E., Love, G.D., 2006. Compositional differences
666   in biomarker constituents of the hydrocarbon, resin, asphaltene and kerogen
667   fractions: An example from the Jet Rock (Yorkshire, UK). Org. Geochem. 37, 369–
668   383.
669   Bradshaw, M J, J C W Cope, D W Cripps, D T Donovan, M K Howarth, P F Rawson, I
670   M West, and W A Wimbledon. 1992. "Jurassic." Geol. Soc., London, Memoirs 13,
671   107–129.
672   Brocks, J., Love, G., Summons, R., Knoll, A., Logan, G., Bowden, S., 2005. Biomarker
673   evidence for green and purple sulphur bacteria in a stratified Palaeoproterozoic sea.
674   Nature 437, 866–870.
675   Brocks, J., Schaeffer, P., 2008. Okenane, a biomarker for purple sulfur bacteria
676   (Chromatiaceae), and other new carotenoid derivatives from the 1640 Ma Barney
677   Creek Formation. Geochim. Cosmochim. Acta 72, 1396–1414.
678   Brocks, J.J., Summons, R.E., 2003. Sedimentary hydrocarbons, biomarkers for early life.
679   In: Treatise on Geochemistry, (Elsevier-Pergamon, Oxford). Chpt. 8.03, pp. 63–115.
680   Brüchert, V., Jørgensen, B.B., Neumann, K., Riechmann, D., Schlösser, M., Schulz, H.,
681   2003. Regulation of bacterial sulfate reduction and hydrogen sulfide fluxes in the
682   central Namibian coastal upwelling zone. Geochim. Cosmochim. Acta 67, 4505–
683   4518.
684   Burdige, D., 2007. Preservation of organic matter in marine sediments: controls,
685   mechanisms, and an imbalance in sediment organic carbon budgets? Chem. Rev.

686   107, 467–485.

687 Bühring, S., Sievert, S., Jonkers, H., Ertefai, T., Elshahed, M., Krumholz, L., Hinrichs, K.
688   -U., 2011. Insights into chemotaxonomic composition and carbon cycling of
689   phototrophic communities in an artesian sulfur-rich spring (Zodletone, Oklahoma,
690   USA), a possible analog for ancient microbial mat systems. Geobiol. 9, 166–179.

691 Canfield, D.E., Stewart, F.J., Thamdrup, B., De Brabandere, L., Dalsgaard, T., Delong,
692   E.F., Revsbech, N.P., Ulloa, O., 2010. A Cryptic Sulfur Cycle in Oxygen-Minimum-
693   Zone Waters off the Chilean Coast. Science 330, 1375–1378.

694 Cao, C., Love, G.D., Hays, L., Wang, W., Shen, S., Summons, R.E., 2009.
695   Biogeochemical evidence for euxinic oceans and ecological disturbance presaging
696   the end-Permian mass extinction event. Earth Planet. Sci. Lett. 281, 188–201.

697 Caruthers, A.H., Gröcke, D.R., Smith, P.L., 2011. The significance of an Early Jurassic
698   (Toarcian) carbon-isotope excursion in Haida Gwaii (Queen Charlotte Islands),
699   British Columbia, Canada. Earth Planet. Sci. Lett. 307, 19–26.

700 Caumette, P., Baulaigue, R., Matheron, R., 1991. *Thiocapsa halophila* sp. nov., a new
701   halophilic phototrophic purple sulfur bacterium. Arch. Microbiol. 155, 170–176.

702 Caumette, P., Guyoneaud, R., Imhoff, J., Süling, J., Gorlenko, V., 2004. *Thiocapsa*
703   *marina* sp. nov., a novel, okenone-containing, purple sulfur bacterium isolated from
704   brackish coastal and marine environments. Int. J. Syst. Evol. Microbiol. 54, 1031–
705   1036.

706 Clayton, C., 1991. Effect of maturity on carbon isotope ratios of oils and condensates.
707   Org. Geochem. 17, 887–899.

708 Clayton, C., Bjorøy, M., 1994. Effect of maturity on $^{13}C/^{12}C$ ratios of individual
709   compounds in North Sea oils. Org. Geochem. 21, 737–750.

710 Cohen, A.S., Coe, A.L., Harding, S.M., Schwark, L., 2004. Osmium isotope evidence for
711   the regulation of atmospheric CO_2 by continental weathering. Geology 32, 157–160.

712 Courtillot, V.E., Renne, P.R., 2003. On the ages of flood basalt events. C. R. Geoscience
713   335, 113–140.

714 Dahl, J., Moldowan, J., M., Sundararaman, P., 1993. Relationship of biomarker
715   distribution to depositional environment: Phosphoria Formation, Montana, USA.
716   Org. Geochem. 20, 1001–1017.

717 Didyk, B., Simoneit, B., Brassell, S., Eglinton, G., 1978. Organic geochemical indicators
718   of palaeoenvironmental conditions of sedimentation. Nature 272, 216-222.

719 Dugdale, R., Goering, J., Barber, R., Smith, R., Packard, T., 1977. Denitrification and
720   hydrogen sulfide in the Peru upwelling region during 1976. Deep-Sea Res. 24, 601–
721   608.

722 Eglinton, G., Hamilton, R., 1967. Leaf epicutular waxes. Science. 156, 1322-1335.

723 Ellis, L., Singh, R.K., Alexander, R., Kagi, R.I., 1996. Formation of isohexyl
724   alkylaromatic hydrocarbons from aromatization-rearrangement of terpenoids in the
725   sedimentary environment: A new class of biomarker. Geochim. Cosmochim. Acta
726   60, 4747–4763.

727 Erba, E., 2004. Calcareous nannofossils and Mesozoic oceanic anoxic events. Mar.
728   Micropaleontol. 52, 85–106.

729 Farrimond, P., Eglinton, G., Brassell, S., Jenkyns, H., 1989. Toarcian anoxic event in
730   Europe: an organic geochemical study. Mar. Petrol. Geol. 6, 136–147.

731 Farrimond, P., Stoddart, D., Jenkyns, H., 1994. An Organic Geochemical Profile of the

732   Toarcian Anoxic Event in Northern Italy. Chem. Geol. 111, 17–33.

733 Farrimond, P., Talbot, H.M., Watson, D.F., Schulz, L.K., Wilhelms, A., 2004.
734   Methylhopanoids: Molecular indicators of ancient bacteria and a petroleum
735   correlation tool. Geochim. Cosmochim. Acta 68, 3873–3882.

736 Finkelstein, D.B., Pratt, L.M., Brassell, S.C., 2006. Can biomass burning produce a
737   globally significant carbon-isotope excursion in the sedimentary record? Earth
738   Planet. Sci. Lett. 250, 501–510.

739 Finkelstein, D.B., Pratt, L.M., Curtin, T.M., Brassell, S.C., 2005. Wildfires and seasonal
740   aridity recorded in Late Cretaceous strata from south-eastern Arizona, USA.
741   Sedimentology 52, 587–599.

742 French, K.L., Tosca, N.J., Cao, C., Summons, R.E., 2012. Diagenetic and detrital origin
743   of moretane anomalies through the Permian–Triassic boundary. Geochim.
744   Cosmochim. Acta 84, 104–125.

745 George, S.C., 1992. Effect of igneous intrusion on the organic geochemistry of a siltstone
746   and an oil shale horizon in the Midland Valley of Scotland. Org. Geochem. 18, 705–
747   723.

748 Ghadeer, S.G., Macquaker, J.H.S., 2011. Sediment transport processes in an ancient mud-
749   dominated succession: a comparison of processes operating in marine offshore
750   settings and anoxic basinal environments. J. Geol. Soc. (London) 168, 1121–1132.

751 Grice, K., Backhouse, J., Alexander, R., Marshall, N., Logan, G.A., 2005. Correlating
752   terrestrial signatures from biomarker distributions, δ^{13}C, and palynology in fluvio-
753   deltaic deposits from NW Australia (Triassic–Jurassic). Org. Geochem. 36, 1347–
754   1358.

755 Grice, K., Nabbefeld, B., Maslen, E., 2007. Source and significance of selected
756   polycyclic aromatic hydrocarbons in sediments (Hovea-3 well, Perth Basin, Western
757   Australia) spanning the Permian-Triassic boundary. Org. Geochem. 38, 1795–1803.

758 Gröcke, D., Hori, R., Trabucho-Alexandre, J., Kemp, D., Schwark, L., 2011. An open
759   marine record of the Toarcian oceanic event. Solid Earth 2, 245–257.

760 Handley, L., Talbot, H.M., Cooke, M.P., Anderson, K.E., Wagner, T., 2010.
761   Bacteriohopanepolyols as tracers for continental and marine organic matter supply
762   and phases of enhanced nitrogen cycling on the late Quaternary Congo deep sea fan.
763   Org. Geochem. 41, 910–914.

764 Heimhofer, U., P. A. Hochuli, S. Burla, J. M. L. Dinis, and H. Weissert., 2005. Timing of
765   Early Cretaceous angiosperm diversification and possible links to major
766   paleoenvironmental change. Geology 33, 141-144.

767 Hesselbo, S., 2008. Sequence stratigraphy and inferred relative sea-level change from the
768   onshore British Jurassic. P. Geologist Assoc. 119, 19–34.

769 Hesselbo, S., Jenkyns, H., 1995. A comparison of the Hettangian to Bajocian successions
770   of Dorset and Yorkshire, in: Taylor, P. (Ed.), Field Geology of the British Jurassic.
771   Geological Society of London, pp. 105–150.

772 Hesselbo, S.P., Gröcke, D.R., Jenkyns, H.C., Bjerrum, C.J., Farrimond, P., Morgans Bell,
773   H.S., Green, O.R., 2000. Massive dissociation of gas hydrate during a Jurassic
774   oceanic anoxic event. Nature 406, 392–395.

775 Hesselbo, S.P., Jenkyns, H.C., Duarte, L.V., Oliveira, L.C.V., 2007. Carbon-isotope
776   record of the Early Jurassic (Toarcian) Oceanic Anoxic Event from fossil wood and
777   marine carbonate (Lusitanian Basin, Portugal). Earth Planet. Sci. Lett. 253, 455–470.

778   Hites, R.A., Laflamme, R.E., Farrington, J.W., 1977. Sedimentary Polycyclic Aromatic
779   Hydrocarbons: The Historical Record. Science 198, 829–831.
780   Howarth, M., 1992. The ammonite family Hildoceratidae in the Lower Jurassic of
781   Britain. Palaeontogr. Soc. Monogr. 145, 1–106.
782   Jenkyns, H., 1988. The early Toarcian (Jurassic) anoxic event: stratigraphic, sedimentary,
783   and geochemical evidence. Am. J. Sci. 288, 101–151.
784   Jenkyns, H., Gröcke, D., Hesselbo, S., 2001. Nitrogen isotope evidence for water mass
785   denitrification during the early Toarcian (Jurassic) oceanic anoxic event.
786   Paleoceanography 16, 593–603.
787   Jenkyns, H.C., 1980. Cretaceous anoxic events: from continents to oceans. J. Geol. Soc.
788   (London) 137, 171–188.
789   Jenkyns, H.C., 2010. Geochemistry of oceanic anoxic events. Geochem. Geophys.
790   Geosyst. 11, Q03004.
791   Jiang, C., Alexander, R., Kagi, R.I., Murray, A.P., 1998. Polycyclic aromatic
792   hydrocarbons in ancient sediments and their relationships to palaeoclimate. Org.
793   Geochem. 29, 1721–1735.
794   Jiang, C., Alexander, R., Kagi, R.I., Murray, A.P., 2000. Origin of perylene in ancient
795   sediments and its geological significance. Org. Geochem. 31, 1545–1559.
796   Kawka, O.E., Simoneit, B.R.T., 1990. Polycyclic aromatic hydrocarbons in hydrothermal
797   petroleums from the Guaymas Basin spreading center. Appl. Geochem. 5, 17–27.
798   Kemp, D.B., Coe, A.L., Cohen, A.S., Schwark, L., 2005. Astronomical pacing of
799   methane release in the Early Jurassic period. Nature 437, 396–399.
800   Kemp, D.B., Coe, A.L., Cohen, A.S., Weedon, G.P., 2011. Astronomical forcing and
801   chronology of the early Toarcian (Early Jurassic) oceanic anoxic event in Yorkshire,
802   UK. Paleoceanography 26, PA4210.
803   Kiessling, W., Simpson, C., 2011. On the potential for ocean acidification to be a general
804   cause of ancient reef crises. Glob. Change Biol. 17, 56–67.
805   Killops, S.D., Massoud, M.S., 1992. Polycyclic aromatic hydrocarbons of pyrolytic
806   origin in ancient sediments: evidence for Jurassic vegetation fires. Org. Geochem. 18,
807   1–7.
808   Köster, J., van Kaam-Peters, H., Koopmans, M., de Leeuw, J., Sinninghe Damsté, J.,
809   1997. Sulphurisation of homohopanoids: Effects on carbon number distribution,
810   speciation, and 22S/22R epimer ratios. Geochim. Cosmochim. Acta 61, 2431–2452.
811   Kruge, M.A., Stankiewicz, B.A., Crelling, J.C., Montanari, A., Bensley, D.F., 1994.
812   Fossil charcoal in Cretaceous-Tertiary boundary strata: Evidence for catastrophic
813   firestorm and megawave. Geochim. Cosmochim. Acta 58, 1393–1397.
814   Kuypers, M.M.M., van Breugel, Y., Schouten, S., Erba, E., Sinninghe Damsté, J.S., 2004.
815   N_2-fixing cyanobacteria supplied nutrient N for Cretaceous oceanic anoxic events.
816   Geology 32, 853.
817   Lentz, S.J., Fewings, M.R., 2012. The Wind- and Wave-Driven Inner-Shelf Circulation.
818   Annu. Rev. Marine. Sci. 4, 317–343.
819   Luo, G., Wang, Y., Algeo, T.J., Kump, L.R., Bai, X., Yang, H., Yao, L., Xie, S., 2011.
820   Enhanced nitrogen fixation in the immediate aftermath of the latest Permian marine
821   mass extinction. Geology 39, 647–650.
822   Macquaker, J., Bentley, S.J., Bohacs, K.M., 2010. Wave-enhanced sediment-gravity
823   flows and mud dispersal across continental shelves: Reappraising sediment transport

824   processes operating in ancient mudstone successions. Geology 38, 947-950.

825   Macquaker, J., Taylor, K., 1996. A sequence stratigraphic interpretation of a mudstone-

826   dominated succession: the Lower Jurassic Cleveland Ironstone Formation. J. Geol.

827   Soc. (London) 153, 759–770.

828   Marynowski, L., Simoneit, B.R.T., 2009. Widespread Upper Triassic to Lower Jurassic

829   wildfire records from Poland: Evidence from charcoal and pyrolytic polycyclic

830   aromatic hydrocarbons. Palaios 24, 285–298.

831   McElwain, J.C., Wade-Murphy, J., Hesselbo, S.P., 2005. Changes in carbon dioxide

832   during an oceanic anoxic event linked to intrusion into Gondwana coals. Nature 435,

833   479–482.

834   Meyer, K.M., Macalady, J.L., Fulton, J.M., Kump, L.R., Schaperdoth, I., Freeman, K.H.,

835   2011. Carotenoid biomarkers as an imperfect reflection of the anoxygenic

836   phototrophic community in meromictic Fayetteville Green Lake. Geobiol. 9, 321–

837   329.

838   Moldowan, J.M., Sundararaman, P., Schoell, M., 1986. Sensitivity of biomarker

839   properties to depositional environment and/or source input in the Lower Toarcian of

840   SW-Germany. Org. Geochem. 10, 915–926.

841   Moldowan, J.M., Seifert, W.K., Gallegos, E.J., 1985. Relationship Between Petroleum

842   Composition and Depositional Environment of Petroleum Source Rocks. Am. Assoc.

843   Petr. Geol. B. 69, 1255–1268.

844   Naeher, S., Geraga, M., Papatheodorou, G., Ferentinos, G., Kaberi, H., Schubert, C. J.,

845   2012. Environmental variations in a semi-enclosed embayment (Amvrakikos Gulf,

846   Greece)- reconstructions based on benthic foraminifera abundance and lipid

847   biomarker pattern. Biogeosciences 9, 5081-5094.

848   Naqvi, S., Naik, H., Pratihary, A., D'Souza, W., Narvekar, P., Jayakumar, D., Devol, A.,

849   Yoshinari, T., Saino, T., 2006. Coastal versus open-ocean denitrification in the

850   Arabian Sea. Biogeosciences 3, 621–633.

851   Noble, R.A., Alexander, R., Kagi, R.I., Knox, J., 1986. Identification of some diterpenoid

852   hydrocarbons in petroleum. Org. Geochem. 10, 825–829.

853   O'Brien, N., 1990. Significance of lamination in Toarcian (Lower Jurassic) shales from

854   Yorkshire, Great Britain. Sediment. Geol. 67, 25–34.

855   Pálfy, J., Smith, P., 2000. Synchrony between Early Jurassic extinction, oceanic anoxic

856   event, and the Karoo-Ferrar flood basalt volcanism. Geology 28, 747–750.

857   Pancost, R., Crawford, N., Magness, S., Turner, A., Jenkyns, H., Maxwell, J., 2004.

858   Further evidence for the development of photic-zone euxinic conditions during

859   Mesozoic oceanic anoxic events. J. Geol. Soc. (London) 161, 353–364.

860   Pancost, R., Freeman, K., Patzkowsky, M., 1999. Organic-matter source variation and the

861   expression of a late Middle Ordovician carbon isotope excursion. Geology 27, 1015–

862   1018.

863   Peters, K.E., Walters, C.C., Moldowan, J.M., 2005. The Biomarker Guide: Biomarkers

864   and Isotopes In Petroleum Systems and Earth History, 2nd ed, The Biomarker Guide:

865   Biomarkers and Isotopes in Petroleum Systems and Earth History. Cambridge

866   University Press.

867   Powell, J.H., 2010. Jurassic sedimentation in the Cleveland Basin: a review. Proc. Yorks.

868   Geol. Soc. 58, 21–72.

869   Prauss, M., Ligouis, B., Luterbacher, H., 1991. Organic matter and palynomorphs in the

870   "Posidonienschiefer" (Toarcian, Lower Jurassic) of southern Germany. Geol. Soc.,
871   London Spec. Publ. 58, 335–351.
872 Rashby, S., Sessions, A.L., Summons, R.E., Newman, D., 2007. Biosynthesis of 2-
873   methylbacteriohopanepolyols by an anoxygenic phototroph. Proc. Natl. Acad. Sci.
874   U.S.A 104, 15099.
875 Röhl, H., Schmid, A., Oschmann, W., Frimmel, A., Schwark, L., 2001. The Posidonia
876   Shale (Lower Toarcian) of SW-Germany: an oxygen-depleted ecosystem controlled
877   by sea level and palaeoclimate. Palaeogeogr. Palaeoclimatol. Palaeoecol. 165, 27–52.
878 Sabatino, N., Neri, R., Bellanca, A., Jenkyns, H.C., Baudin, F., Parisi, G., Masetti, D.,
879   2009. Carbon-isotope records of the Early Jurassic (Toarcian) oceanic anoxic event
880   from the Valdorbia (Umbria-Marche Apennines) and Monte Mangart (Julian Alps)
881   sections: palaeoceanographic and stratigraphic implications. Sedimentology 56,
882   1307–1328.
883 Sãenz, J.P., Eglinton, T.I., Summons, R.E., 2011. Abundance and structural diversity of
884   bacteriohopanepolyols in suspended particulate matter along a river to ocean transect.
885   Org. Geochem. 42, 774–780.
886 Schlanger, S.O., Jenkyns, H.C., 1976. Cretaceous oceanic anoxic events: causes and
887   consequences. Geol. Mijnbouw 55, 179–184.
888 Schouten, S., van Kaam-Peters, H., Rijpstra, W., Schoell, M., Sinninghe Damsté , J.,
889   2000. Effects of an oceanic anoxic event on the stable carbon isotopic composition of
890   Early Toarcian carbon. Am. J. Sci. 300, 1–22.
891 Schouten, S., Woltering, M., Rijpstra, W.I.C., Sluijs, A., Brinkhuis, H., Sinninghe
892   Damsté, J.S., 2007. The Paleocene–Eocene carbon isotope excursion in higher plant
893   organic matter: Differential fractionation of angiosperms and conifers in the Arctic.
894   Earth Planet. Sci. Lett. 258, 581–592.
895 Schunck, H., Lavik, G., Desai, D.K., Großkopf, T., Kalvelage, T., Löscher, C.R.,
896   Paulmier, A., Contreras, S., Siegel, H., Holtappels, M., Rosenstiel, P., Schilhabel,
897   M.B., Graco, M., Schmitz, R.A., Kuypers, M.M.M., LaRoche, J., 2013. Giant
898   Hydrogen Sulfide Plume in the Oxygen Minimum Zone off Peru Supports
899   Chemolithoautotrophy. PLoS One 8, e68661.
900 Schwark, L., Frimmel, A., 2004. Chemostratigraphy of the Posidonia Black Shale, SW-
901   Germany. Chem. Geol. 206, 231–248.
902 Sephton, M.A., Love, G.D., Meredith, W., Snape, C.E., Sun, C.-G., Watson, J.S., 2005.
903   Hydropyrolysis: A new technique for the analysis of macromolecular material in
904   meteorites. Planet. Space Sci. 53, 1280–1286.
905 Sepúlveda, J., Wendler, J., Leider, A., Kuss, H–J., Summons, R.E., Hinrichs, K–U., 2009.
906   Molecular isotopic evidence of environmental and ecological changes across the
907   Cenomanian–Turonian boundary in the Levant Platform of central Jordan. Org.
908   Geochem. 40, 553–568.
909 Sinninghe Damsté, J.S., Schouten, S., Biological markers for anoxia in the photic zone of
910   the water column. In: The Handbook of Environmental Chemistry, (Springer-Verlag,
911   Berlin), pp. 127–163.
912 Sinninghe Damsté, J., Kenig, F., Koopmans, M., Köster, J., Schouten, S., Hayes, J., de
913   Leeuw, J., 1995. Evidence for gammacerane as an indicator of water column
914   stratification. Geochim. Cosmochim. Acta 59, 1895–1900.
915 Smith, F., Wing, S., Freeman, K., 2007. Magnitude of the carbon isotope excursion at the

916   Paleocene–Eocene thermal maximum: The role of plant community change. Earth
917   Planet. Sci. Lett. 262, 50–65.
918 Smittenberg, R.H., Pancost, R.D., Hopmans, E.C., Paetzel, M., and Sinninghe Damsté,
919   J.S., 2004, A 400-year record of environmental change in an euxinic fjord as revealed
920   by the sedimentary biomarker record: Palaeogeogr. Palaeoclimatol. Palaeoecol. 202,
921   331–351.
922 Stewart, F.J., Ulloa, O., DeLong, E.F., 2012. Microbial metatranscriptomics in a
923   permanent marine oxygen minimum zone. Environ. Microbiol. 14, 23–40.
924 Suan, G., Nikitenko, B.L., Rogov, M.A., Baudin, F., Spangenberg, J.E., Knyazev, V.G.,
925   Glinskikh, L.A., Goryacheva, A.A., Adatte, T., Riding, J.B., Föllmi, K.B., Pittet, B.,
926   Mattioli, E., Lécuyer, C., 2011. Polar record of Early Jurassic massive carbon
927   injection. Earth Planet. Sci. Lett. 312, 102–113.
928 Suan, G., Pittet, B., Bour, I., Mattioli, E., Duarte, L., Mailliot, S., 2008. Duration of the
929   Early Toarcian carbon isotope excursion deduced from spectral analysis:
930   Consequence for its possible causes. Earth Planet. Sci. Lett. 267, 666–679.
931 Summons, R.E., Jahnke, L., Hope, J., Logan, G., 1999. 2-Methylhopanoids as biomarkers
932   for cyanobacterial oxygenic photosynthesis. Nature 23, 85–88.
933 Talbot, H., Farrimond, P., 2007. Bacterial populations recorded in diverse sedimentary
934   biohopanoid distributions. Org. Geochem. 38, 1212–1225.
935 Talbot, H.M., Watson, D.F., Pearson, E.J., Farrimond, P., 2003. Diverse biohopanoid
936   compositions of non-marine sediments. Org. Geochem. 34, 1353–1371.
937 Talbot, M., Livingstone, D., 1989. Hydrogen Index and Carbon Isotopes of Lacustrine
938   Organic-Matter as Lake Level Indicators. Palaeogeogr. Palaeoclimatol. Palaeoecol.
939   70, 121–137.
940 Tang, Y., Huang, Y., Ellis, G.S., Wang, Y., Kralert, P.G., Gillaizeau, B., Ma, Q., Hwang,
941   R., 2005. A kinetic model for thermally induced hydrogen and carbon isotope
942   fractionation of individual n-alkanes in crude oil. Geochim. Cosmochim. Acta 69,
943   4505–4520.
944 ten Haven, H., Rohmer, M., Rullkötter, J., Bisseret, P., 1989. Tetrahymanol, the most
945   likely precursor of gammacerane, occurs ubiquitously in marine sediments. Geochim.
946   Cosmochim. Acta 53, 3073–3079.
947 Trabucho-Alexandre, J., Dirkx, R., Veld, H., Klaver, G., de Boer, P., 2012. Toarcian
948   Black Shales in the Dutch Central Graben: Record of Energetic, Variable
949   Depositional Conditions during an Oceanic Anoxic Event. J. Sediment. Res. 82, 104-
950   120.
951 Trabucho-Alexandre, J., Tuenter, E., Henstra, G., van der Zwan, K., van de Wal, R.,
952   Dijkstra, H., de Boer, P., 2010. The mid-Cretaceous North Atlantic nutrient trap:
953   Black shales and OAEs. Paleoceanography 25, PA4201.
954 van Breugel, Y., Baas, M., Schouten, S., Mattioli, E., Sinninghe Damsté, J.S., 2006.
955   Isorenieratane record in black shales from the Paris Basin, France: Constraints on
956   recycling of respired CO_2 as a mechanism for negative carbon isotope shifts during
957   the Toarcian oceanic anoxic event. Paleoceanography 21, PA4220.
958 van de Schootbrugge, B., McArthur, J.M., Bailey, T.R., Rosenthal, Y., Wright, J.D.,
959   Miller, K.G., 2005. Toarcian oceanic anoxic event: An assessment of global causes
960   using belemnite C isotope records. Paleoceanography 20, PA3008.
961 Venkatesan, M.I., Dahl, J., 1989. Organic geochemical evidence for global fires at the

962   Cretaceous/Tertiary boundary. Nature 338, 57–60.

963 Vetö, I., Demeny, A., Hertelendi, E., Hetenyi, M., 1997. Estimation of primary
964   productivity in the Toarcia Tethys- a novel approach based on TOC, reduced sulphur
965   and manganese contents. Palaeogeogr. Palaeoclimatol. Palaeoecol. 132, 355–371.

966 Wahlund, T., Woese, C., Castenholz, R., Madigan, M., 1991. A thermophilic green sulfur
967   bacterium from New Zealand hot springs, *Chlorobium tepidum* sp. nov. Arch.
968   Microbiol. 156, 81–90.

969 Wakeham, S., Schaffner, C., Giger, W., 1980. Polycyclic aromatic hydrocarbons in
970   Recent lake sediments--I. Compounds having anthropogenic origins. Geochim.
971   Cosmochim. Acta 44, 403–413.

972 Wakeham, S.G., Amann, R., Freeman, K.H., Hopmans, E.C., Jørgensen, B.B., Putnam,
973   I.F., Schouten, S., Sinninghe Damsté, J.S., Talbot, H.M., Woebken, D., 2007.
974   Microbial ecology of the stratified water column of the Black Sea as revealed by a
975   comprehensive biomarker study. Org. Geochem. 38, 2070–2097.

976 Wakeham, S.G., Turich, C., Schubotz, F., Podlaska, A., Li, X., Varela, R., Astor, Y.,
977   Sãenz, J.P, Rush, D., Sinninghe Damsté , J.S., Summons, R.E., Scranton, M.I.,
978   Taylor, G. T., Hinrichs, K.-U., 2012. Biomarkers, chemistry, and microbiology show
979   chemoautotrophy in a multilayer chemocline in the Cariaco Basin. Deep-Sea Res. I
980   163, 133-156.

981 Wen, Z., Ruiyong, W., Radke, M., Qingyu, W., Guoying, S., Zhili, L., 2000. Retene in
982   pyrolysates of algal and bacterial organic matter. Org. Geochem. 31, 757–762.

983 Wignall, P., Newton, R.J., Little, C.T.S., 2005. The timing of paleoenvironmental change
984   and cause-and-effect relationships during the Early Jurassic mass extinction in
985   Europe. Am. J. Sci. 305, 1014–1032.

986 Xie, S., Pancost, R., Yin, H., Wang, H., Evershed, R., 2005. Two episodes of microbial
987   change coupled with Permo/Triassic faunal mass extinction. Nature 434, 494–497.

988 Zhang, C., Zhang, Y., Cai, C., 2011. Aromatic isoprenoids from the 25-65 Ma saline
989   lacustrine formations in the western Qaidam Basin, NW China. Org. Geochem. 42,
990   851-855.

991 Zundel, M., Rohmer, M., 1985. Prokaryotic triterpenoids. 1. 3β-Methylhopanoids from
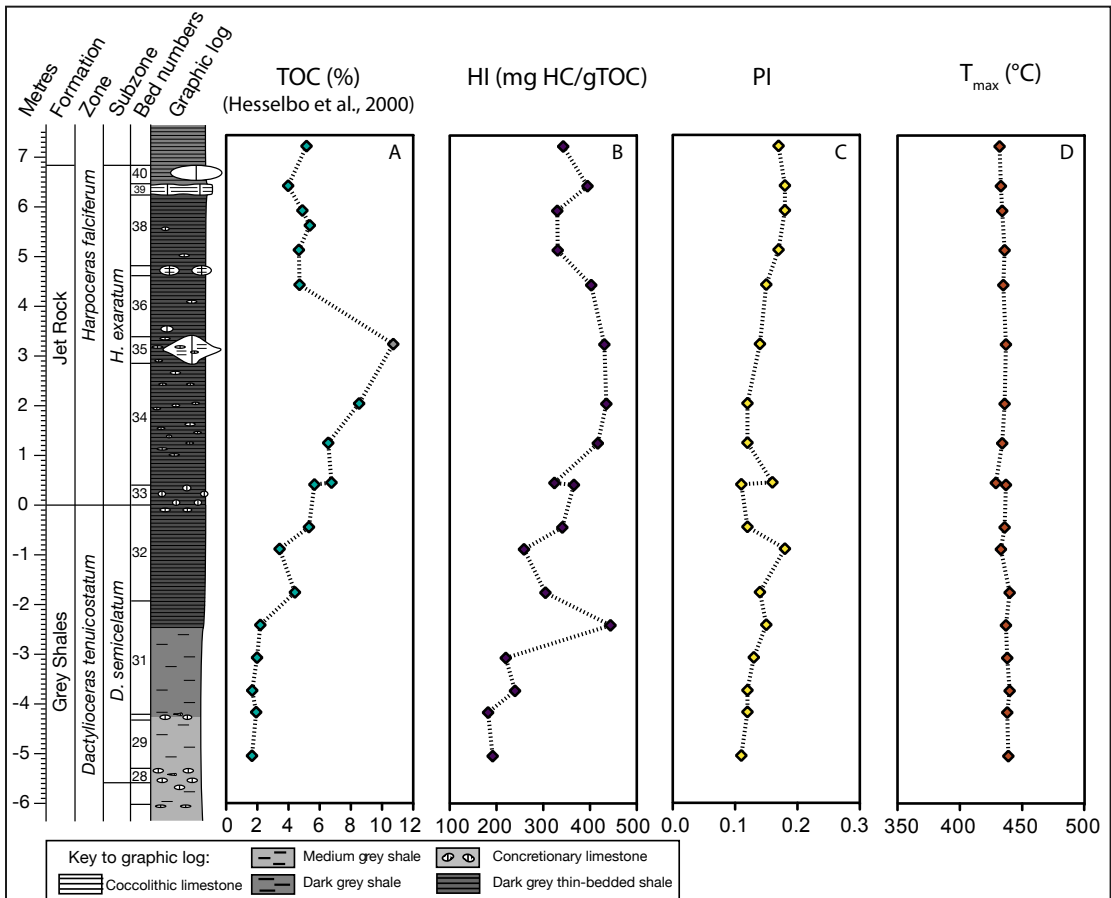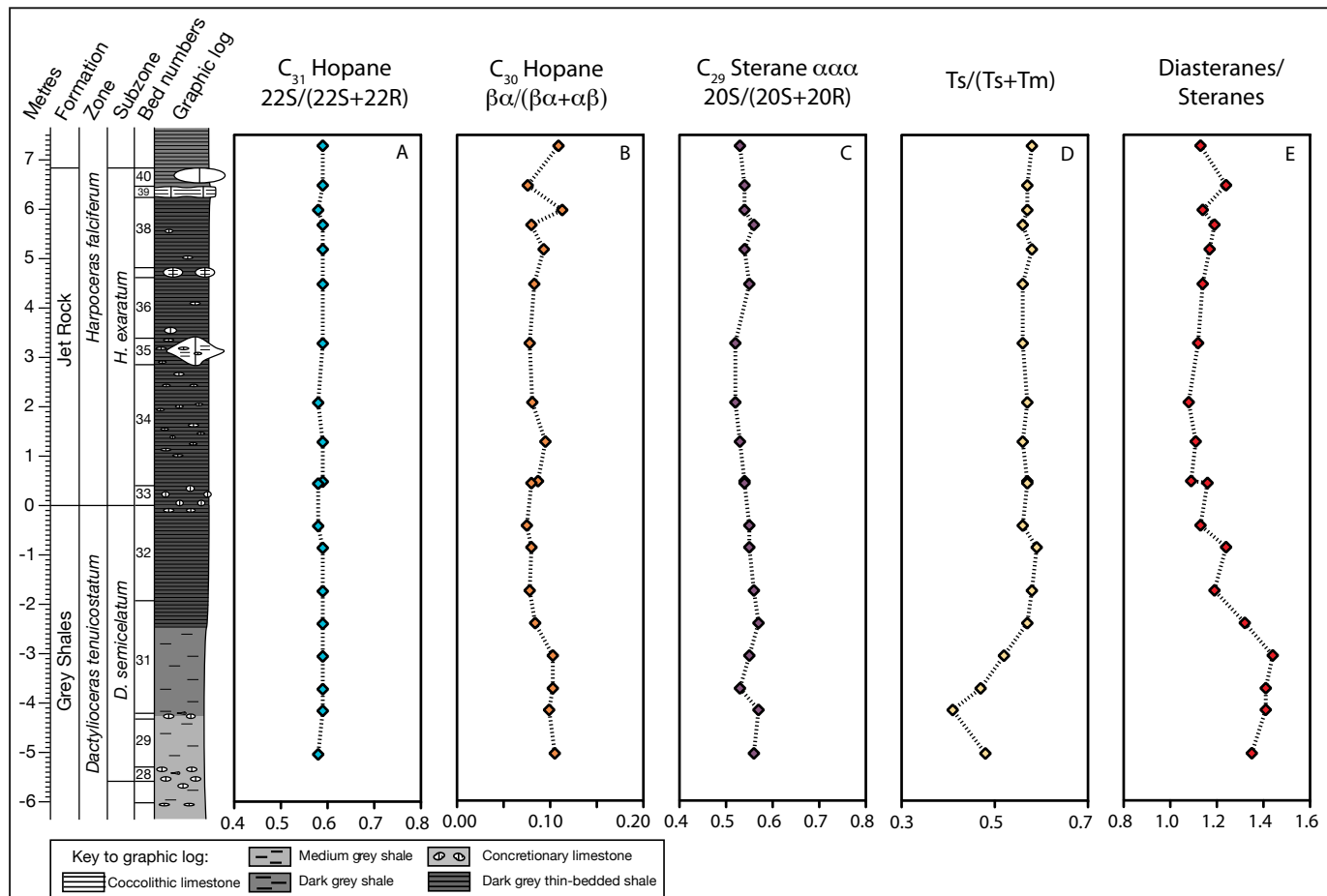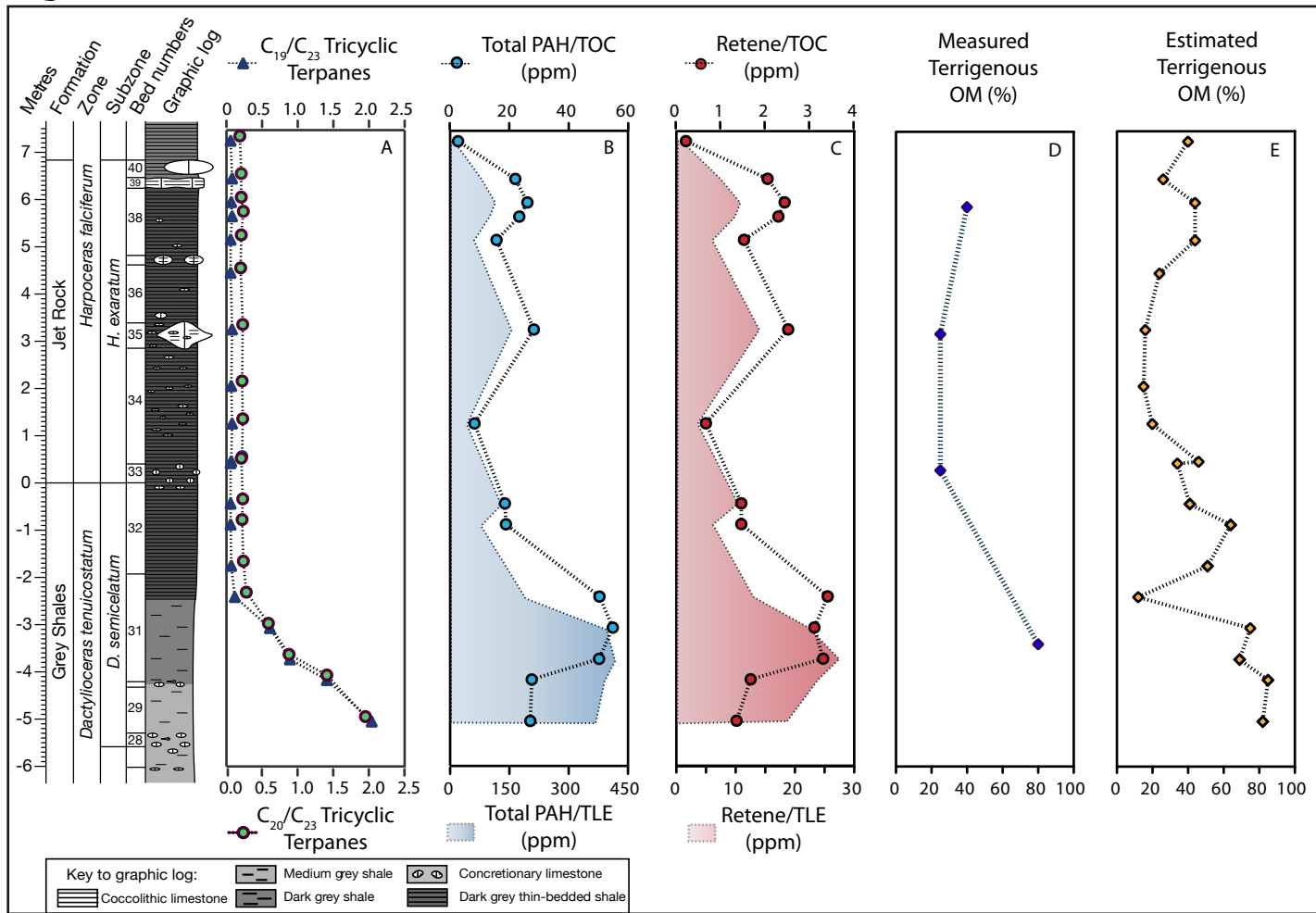992   *Acetobacter* species and *Methylococcus capsulatus*. Eur. J. Biochem. 150, 23–27.
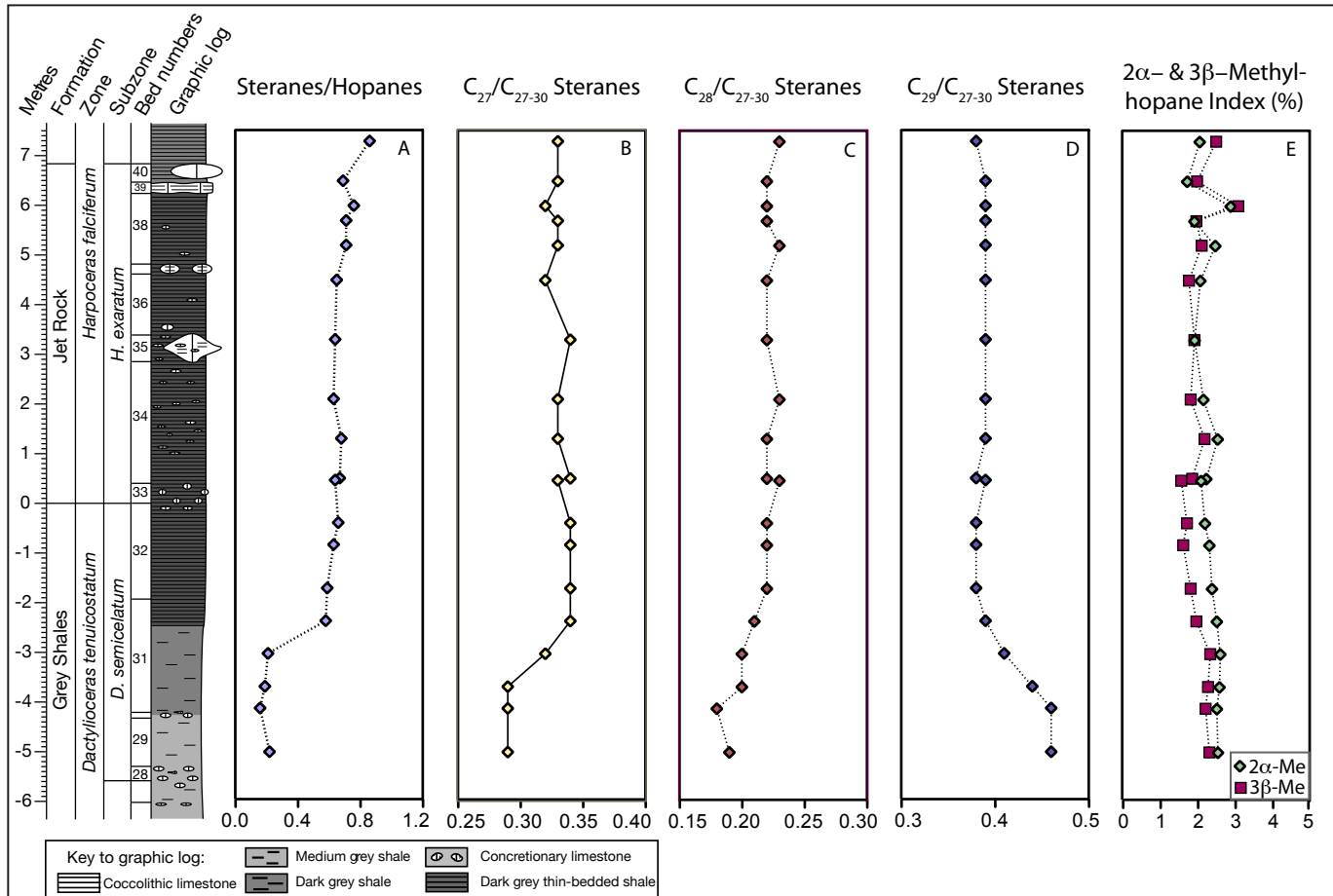
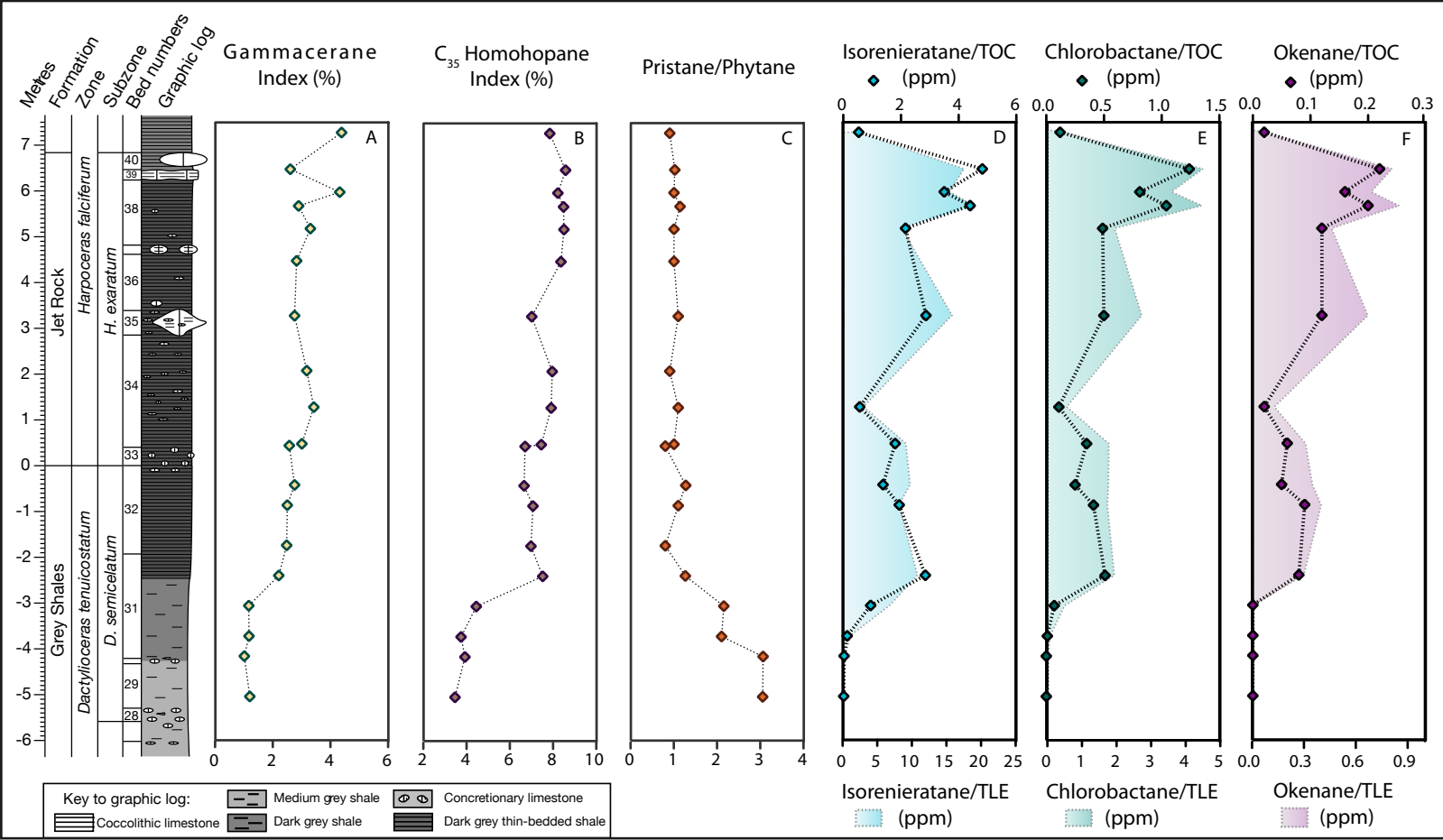993

Figure 1

Figure 2

Figure 3
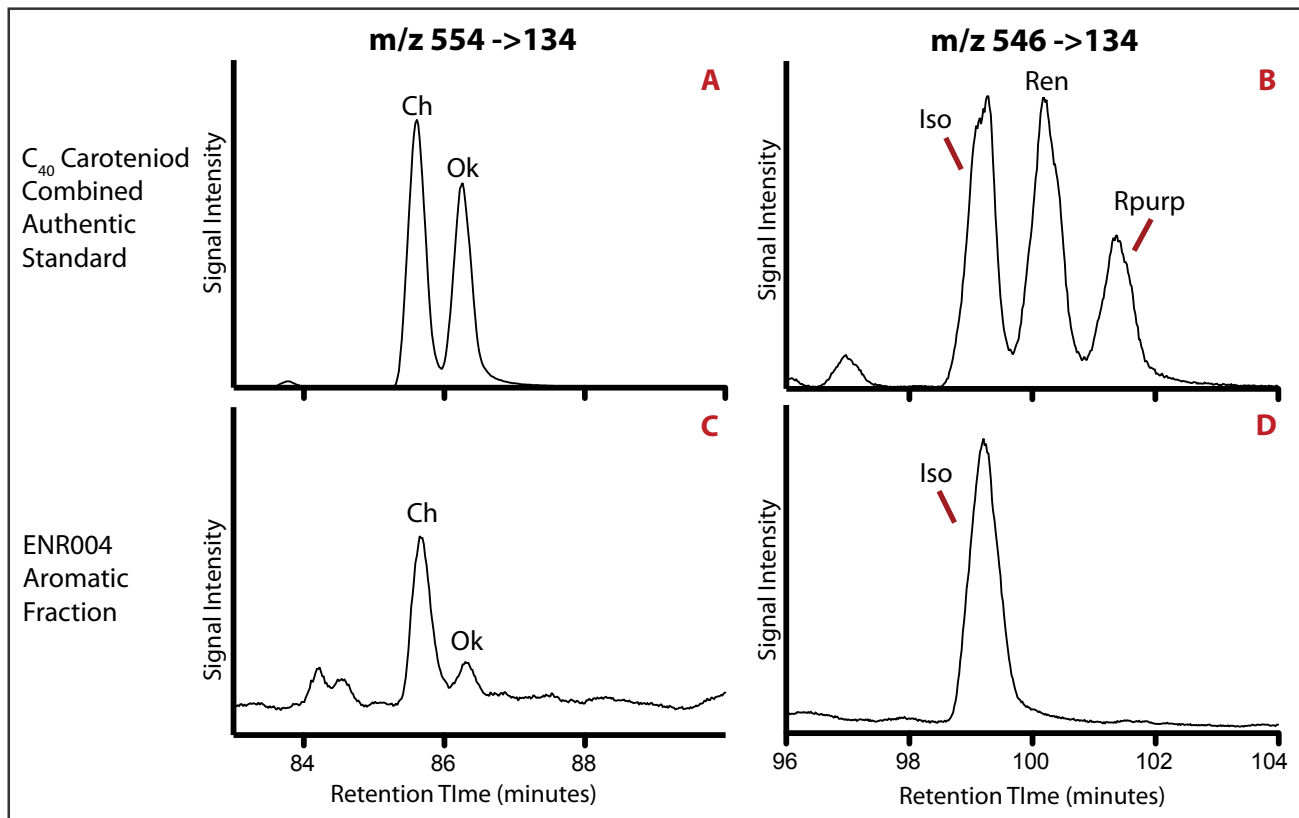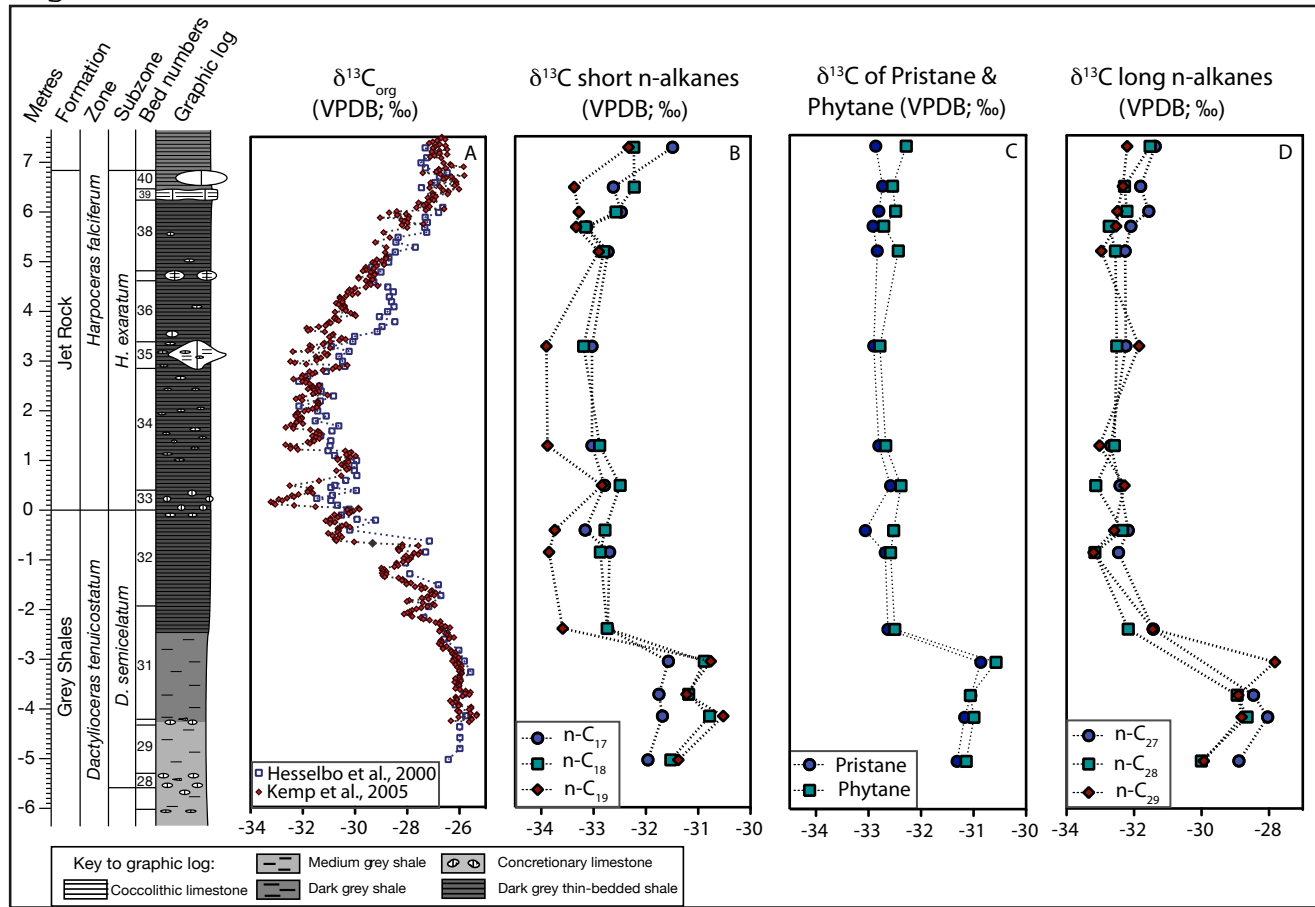
Figure 4

Figure 5

Figure 6

Figure 7

Supplementary Online Material (SOM)

3.1 Rock-Eval pyrolysis

Powdered sediment samples (~1 g) were analyzed at the University of Newcastle on a Rock-Eval pyrolysis instrument. The total organic carbon (TOC %), T_{max} (°C), S_1, and S_2 were determined. The S_1 and S_2 are expressed in mg hydrocarbons (HC) per gram dry rock. These parameters were used to calculate the hydrogen index (HI) (HI=[100*S_2]/TOC; expressed in mg hydrocarbon (HC)/g TOC) and the production index (PI) (PI= S_1/[S_1+S_2]). The Rock-Eval TOC values and the bulk $\delta^{13}C_{org}$ have been previously reported (Hesselbo et al., 2000).

3.2 Organic petrography

In order to examine the nature of the organic matter, particularly the fraction of terrigenous organic matter, four samples across the section were prepared for optical analysis of the kerogen. Kerogen was isolated from the sample material remaining after lipid extraction as described in section 3.3. The mineral matrix was removed by the sequential addition of HCl and HF. Samples were centrifuged and rinsed between acid treatments, and the residual matter was rinsed with water and methanol. A subsample of each kerogen sample was mounted onto a slide in duplicate and assessed optically under white light and fluorescent light using a Zeiss research microscope and a Zeiss x 40 Plan-Neofluar objective. A Zeiss Axioskop, Axio Image D1, and a Zeiss 18 filter set were used to take photomicrographs and fluorescence images.

The fraction of terrigenous organic matter was estimated for the samples that were not analyzed by organic petrography using the linear relationship between the percent terrigenous organic matter measured by optical microscopy and the corresponding HI:

$$f_{Terr\ OM}\ (\%) = -0.279 * HI + 136 \qquad\qquad (1)$$

where the linear regression had an R^2 value of 0.90 and $f_{Terr\ OM}$ represents the terrigenous organic matter as a percentage.

3.3 Biomarker extraction and analysis

Powdered samples (~ 5 g) were extracted using a Dionex ASE 200 Accelerated Solvent Extractor at 1000 psi and 100°C, with a solvent mixture of dichloromethane:methanol 9:1 (v/v). The total lipid extract (TLE) was reacted with acid-activated copper shots to remove elemental sulfur. Asphaltenes were separated (3x) from the maltene fraction by precipitation in n-pentane at 4°C, and after centrifugation at 3000 rpm for 10 minutes. The maltene fraction was then separated into saturated, aromatic, and polar fractions by silica gel chromatography using hexane, 1:1 (v/v) hexane/dichloromethane, and 7:3 (v/v) dichloromethane/methanol.

The saturated fractions were screened by gas chromatography-mass spectrometry (GC-MS) in full scan using an Agilent 6890 GC equipped with a HP6890 autosampler and interfaced to an Agilent 5973 mass spectrometer. Saturated hydrocarbons were also analyzed by gas chromatography-metastable reaction monitoring-mass spectrometry (GC-MRM-MS) on a Micromass Autospec Ultima mass spectrometer coupled with an Agilent 6890N GC. The analysis was carried out with a 60 m J&W Scientific DB-1 fused silica capillary column (internal diameter: 0.25 mm; 0.25 m film thickness) in pulsed splitless mode. The initial GC oven temperature was programmed to 60°C (held for 2

minutes), ramped to 150°C at 10°C/minute, and then to 315°C at 3°C/minute (held for 24 minutes). The ion source was in EI mode at a temperature of 250°C, an ionization energy of 70 eV, and acceleration voltage of 8000 kV. Tricyclic terpanes and hopanes were identified by MRM using the molecular ion to the m/z 191 transitions. Likewise, steranes were identified by MRM using the molecular ion to m/z 217 transitions.

The aromatic fraction was analyzed by GC-MS in SIM modes. Prior to analysis, 400 ng of an aromatic internal standard, deuterated phenanthrene, was added to each sample. The GC was fitted with a DB-5 stationary phase column, and the GC oven temperature was ramped from 60°C to 150°C at 20°C/minute, and then to 330°C at 4°C/minute (held for 27 minutes). The aryl isoprenoids and isorenieratane was identified in the m/z 134 ion chromatograms and quantified using the internal standard. Absolute quantification is not possible without taking into account relative response factors but our approach does allow an internally consistent estimation across the sample set.

The aromatic fraction was also analyzed by GC-MS in full scan and MRM modes on a Micromass Autospec Ultima mass spectrometer coupled with an Agilent 6890N GC autospec. The GC was fitted with a DB-5 stationary phase column. Polycyclic aromatic hydrocarbons (PAHs) were identified and quantified in full scan mode by their mass spectra and by comparison with a mix of authentic standards, with the exception of retene, coronene, and triphenylene, which were identified by their mass spectra and relative retention time. Aromatic carotenoid derivatives were also analyzed by GC-MRM-MS using parent-daughter reactions. Isorenieratane, okenane, and chlorobactane were identified in characteristic MRM transitions by comparison of retention times to an extract from the Barney Creek Formation (BCF) and a standard mix of hydrogenated

carotenoids containing chlorobactane, okenane, isorenieratane, renieratane, and renierapurpane. Using the MRM data, okenane and chlorobactane were quantified against the GC-MSD quantified isorenieratane. The aromatic carotenoid derivative and PAH concentrations were normalized against mass of TLE and TOC.

Compound specific carbon isotopic measurements of saturated hydrocarbons were made by gas chromatography/combustion/ isotope ratio mass spectrometry (GC-C-IRMS) using a Thermo Finnigan Delta plus XP coupled to a Thermo Finnigan Trace GC. The initial oven temperature was programmed to 60°C (held for 3 minutes), ramped to 180°C at 10°C/min, and then to 320°C at 4°C/min (held for 20 minutes). All samples were bracketed by pulses of in house calibrated reference CO_2 gas and Oztech calibrated reference CO_2 gas. A standard mix of n-alkanes (mix A; Arndt Schimmelmann, Indiana University) was analyzed twice a day to monitor the instrument condition. The mean value of triplicate analyses are reported here in permil (‰) relative to Vienna Pee Dee belemnite (VPDB), and the standard deviation from the mean value was better than 0.4‰.